Journal of Molecular Spectroscopy 256 (2009) 256–278

Contents lists available at ScienceDirect

Journal of Molecular Spectroscopy

journal homepage: www.elsevier.com/locate/jms

Stretch-bend combination polyads in the $\tilde{A}^1A_u$ state of acetylene, C_2H_2

Adam H. Steeves [a], Hans A. Bechtel [a,1], Anthony J. Merer [b,c], Nami Yamakita [d], Soji Tsuchiya [e], Robert W. Field [a,*]

[a] Department of Chemistry, Massachusetts Institute of Technology, Room 6-219, Cambridge, MA 02139, USA
[b] Institute of Atomic and Molecular Sciences, Academia Sinica, Taipei 10617, Taiwan
[c] Department of Chemistry, University of British Columbia, Vancouver, BC, Canada V6T 1Z1
[d] Department of Chemical and Biological Sciences, Japan Women's University, Mejirodai, Bunkyo-ku, Tokyo 112-8681, Japan
[e] Department of Applied Chemistry and Institute of Molecular Science, National Chiao Tung University, Hsinchu 30010, Taiwan

ARTICLE INFO

Article history:
Received 13 April 2009
Available online 18 May 2009

Keywords:
Acetylene
Cis–trans isomerization
Vibration–rotation analysis

ABSTRACT

Rotational analyses are reported for a number of newly-discovered vibrational levels of the S_1-*trans* ($\tilde{A}^1A_u$) state of C_2H_2. These levels are combinations where the Franck–Condon active v'_2 and v'_3 vibrational modes are excited together with the low-lying bending vibrations, v'_4 and v'_6. The structures of the bands are complicated by strong *a*- and *b*-axis Coriolis coupling, as well as Darling–Dennison resonance for those bands that involve overtones of the bending vibrations. The most interesting result is the strong anharmonicity in the combinations of v'_3 (*trans* bend, a_g) and v'_6 (in-plane *cis* bend, b_u). This anharmonicity presumably represents the approach of the molecule to the *trans–cis* isomerization barrier, where *ab initio* results have predicted the transition state to be half-linear, corresponding to simultaneous excitation of v'_3 and v'_6. The anharmonicity also causes difficulty in the least squares fitting of some of the polyads, because the simple model of Coriolis coupling and Darling–Dennison resonance starts to break down. The effective Darling–Dennison parameter, K_{4466}, is found to increase rapidly with excitation of v'_3, while many small centrifugal distortion terms have had to be included in the least squares fits in order to reproduce the rotational structure correctly. Fermi resonances become important where the *K*-structures of different polyads overlap, as happens with the $2^13^1B^1$ and 3^1B^3 polyads ($B = 4$ or 6). The aim of this work is to establish the detailed vibrational level structure of the S_1-*trans* state in order to search for possible S_1-*cis* ($^1A_2$) levels. This work, along with results from other workers, identifies at least one *K* sub-level of every single vibrational level expected up to a vibrational energy of 3500 cm^{-1}.

© 2009 Elsevier Inc. All rights reserved.

1. Introduction

The electronic spectrum of acetylene attracts considerable attention because of its many interesting dynamical aspects. Much of the emphasis is on the lowest singlet excited state, S_1 ($\tilde{A}^1A_u$), where *ab initio* calculations [1–6] indicate that there is a comparatively low barrier to *trans–cis* isomerization and, at higher energy, a conical intersection with the second singlet excited state, S_2. Perturbations by triplet states are widespread in the S_1 state [7–14], where the density of such perturbations depends on the specific vibrations that are excited, and the onset of predissociation [15,16] leads to interest in the mechanisms of the near-threshold photodissociation of acetylene [2,3,17,18]. Moreover, the $\tilde{A}^1A_u$–$\tilde{X}$ $^1\Sigma_g^+$ transition is very useful for reaching other regions of the electronic manifold of C_2H_2 by double resonance because it is highly structured and the assignments of the prominent bands are well understood. Many experiments of this type have been carried out in order to characterize the higher vibrational levels of the ground state [19–28], the Rydberg states [29–31], and the ground state of the cation [32,33].

The first rotational analyses of the $\tilde{A}$–$\tilde{X}$ system, over 50 years ago [34–36], showed that C_2H_2, though linear in its ground electronic state, becomes *trans*-bent (point group C_{2h}) in the $\tilde{A}$ state. Consistent with this, the most obvious feature of the vibrational structure in absorption is a long progression in the *trans*-bending vibration, v'_3. Since the transition is a $\pi \rightarrow \pi^*$ excitation there is also a short progression in the C–C stretching vibration, v'_2. The spectrum is fairly simple at the long wavelength end, though at room temperature there are many overlapping hot bands whose great intensities follow from the change of geometry on electronic excitation, in accord with the Franck–Condon principle. At higher energy the spectrum becomes more complicated. The regular progressions of the low energy region become irregular and various new progressions appear. In order to understand them, and to interpret the many dynamical aspects, it is necessary to establish the vibrational

* Corresponding author. Fax: +1 (617) 253 7030.
E-mail address: rwfield@mit.edu (R.W. Field).
[1] Present address: Advanced Light Source Division, Lawrence Berkeley National Laboratory, Berkeley, CA 94720, USA.

0022-2852/$ - see front matter © 2009 Elsevier Inc. All rights reserved.
doi:10.1016/j.jms.2009.05.005

assignments as fully as possible, beginning with the fundamentals and working up to the regions of interest.

The main features of the transition have been described in detail by Watson et al. [37,38] Their spectra, taken at room temperature or cooled at −78 °C in a long-path absorption cell, mapped the Franck–Condon active *gerade* vibrational levels of the $\tilde{A}$ state. Some years later the three *ungerade* fundamentals were established by IR–UV double resonance [39,40], leaving only the ν_1' fundamental (C–H symmetric stretch) not securely assigned. The ν_1' fundamental was finally detected recently [41], using laser-induced fluorescence from a jet-cooled sample, so that all the fundamentals have now been analyzed rotationally.

Earlier jet-cooled experiments [42] showed that the spectra are much richer than had been thought in the previous work, with many weaker bands observable among the main progressions. The weak bands are overtones of the low-lying bending vibrations, ν_4' (torsion, a_u) and ν_6' (in-plane *cis* bend, b_u) together with combinations of these with the *gerade* vibrations. A detailed study of the overtone polyads has now been published [43], using data from one photon excitation spectra and IR–UV double resonance. The purpose of the present paper is to describe some of the combination polyads, which are of particular interest for the dynamics of the *trans–cis* isomerization. The structures of the low-lying combination polyads are sufficiently similar to those of the overtone polyads that secure assignments can be made. Together with levels where only the totally symmetric vibrations are excited [37,38,41], every vibrational level expected for the *trans*-bent $\tilde{A}$ state of C_2H_2 up to a vibrational energy of 3500 cm^{-1} can now be accounted for.

It is found that the combinations of ν_3' and ν_6' are strongly anharmonic [10], which appears to be associated with the approach to the *trans–cis* isomerization barrier. Stanton et al. [1] and Ventura et al. [5] have performed *ab initio* calculations of the isomerization pathway, and conclude that the molecule is half-linear at the barrier, meaning that one of the CCH angles is approximately 180° while the other remains at about 120°. This structure corresponds to simultaneous excitation of the *trans* and *cis* bending vibrations, ν_3' and ν_6', with roughly the same number of quanta in each. The energy at the top of the barrier is calculated to be about 4700 cm^{-1}, relative to the zero-point level. Because the ν_3' and ν_6' fundamental frequencies are comparatively large (1048 and 768 cm^{-1}, respectively), levels near the isomerization barrier might be observable as a result of anharmonic coupling. Although the S_1-*cis* state has electronic symmetry $^1A_2$ (so that transitions to it from the ground state are forbidden), S_1-*cis* state levels that have tunneled through the isomerization barrier and picked up intensity by interaction with nearby *trans* levels may appear, and should be identifiable once all the vibrational levels of the S_1-*trans* state have been established.

2. Experimental details

The spectra reported in this paper were taken using the same techniques as in Ref. [43]. A full description was given there, so that only a summary is needed here.

Because of the *g–u* symmetry properties of the levels, and the perpendicular polarization of the $\tilde{A}$–$\tilde{X}$ transition (where $K' - \ell'' = \pm 1$), four sets of spectra had to be recorded in order to establish the complete patterns of upper state levels with $K' = 0$–2. For the *gerade* vibrational levels of the $\tilde{A}^1A_u$ state, the $K' = 1$ rotational levels could be reached in one-photon jet-cooled laser excitation from the Σ_g^+ ($\ell'' = 0$) ground level of the molecule, while the $K' = 0$ and 2 levels could be reached from the ν_4'' fundamental (Π_g, $\ell'' = 1$) using warmer jet conditions. Similarly, for the *ungerade* vibrational levels, the $K' = 1$ rotational levels could be reached in IR–UV double resonance experiments via the ν_3'' fundamental (Σ_u^+, $\ell'' = 0$), while the $K' = 0$ and 2 levels could be reached via the $\nu_3 + \nu_4''$ or $\nu_1 + \nu_5''$ combination levels (species Π_u, $\ell'' = 1$).

Laser-induced fluorescence spectra of neat acetylene were recorded in an unskimmed free jet expansion from a General Valve series 9 pulsed valve. The orifice diameter was 0.5 mm, and the backing pressure about 200 kPa. The laser radiation was provided by a Lambda Physik 3002E pulsed dye laser, frequency doubled in a β-barium borate crystal. The spectra were detected with a Hamamatsu R331 photomultiplier and frequency calibrated using $^{130}Te_2$ vapor. The warmer jet conditions for the ν_4'' hot bands were obtained by reducing the distance traveled by the molecules before the UV laser excitation from ∼30 to ∼5 mm, and passing the laser beam though the leading edge of the gas pulse, where the effective vibrational temperature is higher.

The IR radiation for the double resonance experiments was provided by difference frequency generation in a $LiNbO_3$ crystal, using a tunable dye laser in the near infra-red (740–790 nm, Lambda-Physik FL 2002) and an injection-seeded Nd:YAG laser (Spectra-Physics PRO-270) operating at 1064 nm. The IR output was amplified in a second $LiNbO_3$ crystal to a pulse energy of approximately 3 mJ, and its frequency monitored using a photoacoustic cell containing 1.3 kPa of acetylene.

3. Theory

Again, a full description of the theory needed for the rotational structure of the bending polyads was given in Ref. [43] so that only a brief account is given here.

The spectra of the ν_4' and ν_6' fundamentals of the $\tilde{A}$ state, recorded by Utz et al. [39] using IR–UV double resonance, showed that these two fundamentals are almost degenerate, with frequencies of 764.9 and 768.3 cm^{-1}, respectively. They are also extremely strongly Coriolis-coupled, both by *a*- and *b*-axis coupling. The overtones suffer in addition from Darling–Dennison resonance [44], where the coupling parameter, K_{4466}, has the unexpectedly large value of −51.68 cm^{-1} [43]. The various couplings have the effect of almost completely invalidating the conventional harmonic oscillator vibrational labels, and destroying the meaning of the projection quantum number *K*. Nevertheless, it is convenient to use a harmonic oscillator-rigid rotator basis for calculations of the rotational structure.

In a signed-*k* basis, the matrix elements of the rotation, Coriolis coupling and Darling–Dennison resonance are

$$\begin{aligned}
\langle v_4\, v_6 J k|H|v_4\, v_6 J k\rangle &= \left[A - \frac{1}{2}(B+C)\right]k^2 + \frac{1}{2}(B+C)J(J+1)\\
\langle v_4\, v_6 J k\pm 2|H|v_4\, v_6 J k\rangle &= \frac{1}{4}(B-C)[J(J+1) - k(k\pm 1)]^{1/2}[J(J+1) - (k\pm 1)(k\pm 2)]^{1/2}\\
\langle v_4+1\, v_6 J k|H|v_4\, v_6+1 J k\rangle &= 2iA\zeta_{46}^{a}\Omega k[(v_4+1)(v_6+1)]^{1/2}\\
\langle v_4+1\, v_6 J k\pm 1|H|v_4\, v_6+1 J k\rangle &= iB\zeta_{46}^{b}\Omega[J(J+1) - k(k\pm 1)]^{1/2}[(v_4+1)(v_6+1)]^{1/2}\\
\langle v_4\, v_6+1 J k|H|v_4+1\, v_6 J k\rangle &= -2iA\zeta_{46}^{a}\Omega k[(v_4+1)(v_6+1)]^{1/2}\\
\langle v_4\, v_6+1 J k\pm 1|H|v_4+1\, v_6 J k\rangle &= -iB\zeta_{46}^{b}\Omega[J(J+1) - k(k\pm 1)]^{1/2}[(v_4+1)(v_6+1)]^{1/2}\\
\langle v_4+2\, v_6-2 J k|H|v_4\, v_6 J k\rangle &= \frac{1}{4}K_{4466}[(v_4+1)(v_4+2)v_6(v_6-1)]^{1/2}\\
\langle v_4-2\, v_6+2 J k|H|v_4\, v_6 J k\rangle &= \frac{1}{4}K_{4466}[v_4(v_4-1)(v_6+1)(v_6+2)]^{1/2}
\end{aligned} \tag{1}$$

where Ω is Mills' abbreviation [45]

$$\Omega = \frac{1}{2}\left[(\nu_4/\nu_6)^{\frac{1}{2}} + (\nu_6/\nu_4)^{\frac{1}{2}}\right] \tag{2}$$

Since ν_4' and ν_6' are so nearly identical, Ω is almost exactly 1. The quantities *A*, *B* and *C* in the first two lines of Eq. (1) are the rotational constants of the vibrational level of interest; in lines 3–6, the quantities $2A\zeta_{46}^{a}$ and $B\zeta_{46}^{b}$ are coupling parameters, which in first approximation are products of the Coriolis zeta constants and the rotational constants, as indicated.

The imaginary terms in the Hamiltonian matrix can be eliminated by multiplying the harmonic oscillator basis functions by a phase factor $(i)^{v_6}$ before converting to an unsigned-K basis. The result is that all elements off-diagonal in the vibrational quantum numbers carry negative signs. Because of the $\Delta k = \pm 1$ matrix elements of the b-axis Coriolis coupling, the final matrices for each J-value factor only into two sub-matrices, which can be given e- and f-symmetry labels. The forms of these matrices have been discussed previously [43].

The various stretching vibrations involved in the combination polyads described in this paper introduce considerable vibrational anharmonicity. As discussed below, this anharmonicity causes the simple model of Eq. (1) to break down, though the basic structures of the polyads are not changed. We have not found a way to extend the model to allow for the anharmonicity, and in our least squares fittings we have had to introduce, somewhat artificially, a number of centrifugal distortion terms and other corrections. These make minor adjustments to the K-structure, of the order of 1–2 cm^{-1}, which then allow the rotational levels to be fitted with reasonable accuracy, though in some cases the values of these parameters are wholly unreasonable. These terms should be considered merely as fitting parameters, with no real physical meaning.

In this paper, we refer to the bending polyads using the notation B^n. This notation means that the sum of the bending quantum numbers, v'_4 and v'_6, for the vibrational levels making up the polyad is n; for example the 2^1B^2 polyad consists of the three vibrational levels 2^14^2, $2^14^16^1$ and 2^16^2.

4. Appearance of the spectra

Fig. 1 presents survey spectra of the $\tilde{A}$–$\tilde{X}$ system of acetylene as observed in jet-cooled excitation. The lower trace is the one-photon excitation spectrum from the ground vibrational level, which shows the $K' = 1$ levels of the Franck–Condon allowed (*gerade*) vibrational levels together with some of the bands involving the bending overtones. These latter are so much weaker than the Franck–Condon allowed bands that they are barely detectable at the long wavelength end of the spectrum. Leading lines show the positions of these vibrational levels. The upper trace shows the *ungerade* vibrational levels, as seen in IR–UV double resonance taken via the P(1) line of the ground state v''_3 fundamental (which populates the $J'' = 0$ level). In this spectrum, every $\tilde{A}$–$\tilde{X}$ vibrational band is reduced to a single R(0) line with $K' = 1$. The spectra are shown at the same horizontal scale, but displaced from each other by the average frequency of the upper state bending vibrations, so that the corresponding Franck–Condon allowed bands in the two spectra are roughly aligned vertically. The IR–UV double resonance spectrum becomes very complicated at about 46000 cm^{-1} and the vibrational assignments at higher energy have not been completed. Some one-photon bands are unavoidably present in these double resonance spectra; these bands appear whenever the frequency of the UV laser happens to coincide with an absorption band. They are marked with asterisks in the figure.

Two points concerning the 3^nB^1 polyads should be noted in Fig. 1, upper trace. First, the splitting between the two members of the polyads increases with excitation of v'_3 and, second, the lower members drop progressively below the corresponding one-photon bands. In these polyads the nominal 3^n6^1 level always lies below the nominal 3^n4^1 level, providing clear evidence that the combinations of v'_3 and v'_6 are highly anharmonic [10]. Both traces in Fig. 1 show how the widths of the polyads, in energy terms, depend on the number of bending quanta that they contain. This is a result of the Darling–Dennison resonance term which, as Eq. (1) shows, has a strong vibrational quantum number dependence.

Some of the low-lying stretch-bend combination polyads of the $\tilde{A}$ state have already been described by other authors. Specifically, Mizoguchi et al. [10] reported analyses of the 3^2B^1 and 3^3B^1 polyads, and quoted unpublished results for the 3^1B^1 polyad. Steeves et al. [41] have also given some details of the 2^1B^2 polyad, since it interacts with the v'_1 fundamental. The present paper reports

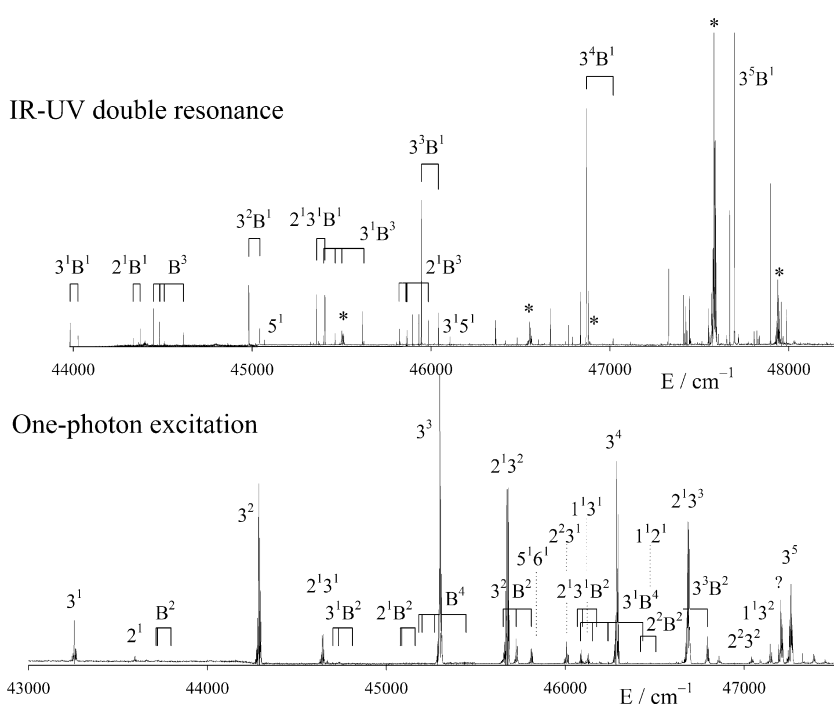

Fig. 1. Survey spectra of the $\tilde{A}$–$\tilde{X}$ system of acetylene recorded with jet-cooling. (Lower trace) One-photon excitation spectrum from the ground vibrational level, showing the $K' = 1$ levels of the Franck–Condon allowed *gerade* vibrational levels and some of the bending overtones. (Upper trace) IR–UV double resonance spectrum of the *ungerade* vibrational levels, taken via the $J'' = 0$ level of the ground state v''_3 fundamental. In this spectrum a vibrational band is reduced to a single $R(0)$, $K' = 1$ line. Asterisks indicate one-photon bands excited by the UV laser alone.

analyses of 2^1B^1, 2^2B^1, 2^2B^2, 3^1B^2, 3^2B^2 and the pairs of interacting polyads $2^13^1B^1/3^1B^3$ and $2^13^1B^2/3^1B^4$. We confirm the conclusion of Mizoguchi et al. [10] that the combinations of ν_3' and ν_6' are strongly anharmonic, though we find that excitation of ν_2' has only a small effect on the structures of the bending polyads.

5. Combination polyads observed in IR–UV double resonance

5.1. The 2^1B^1 polyad (2^14^1 and 2^16^1)

The 2^1B^1 polyad has been observed in IR–UV double resonance, with the IR laser tuned to individual P lines of the ν_3'' IR fundamental ($\ell'' = 0$) to record its $K' = 1$ levels and to the Q branch head of the $\nu_3 + \nu_4''$ combination band ($\ell'' = 1$) to record its $K' = 0$ and 2 levels. A weak Coriolis-induced band going to the lower $K' = 3$ level was also found in the second set of experiments. The Q branch head of the $\nu_3 + \nu_4''$ band is very compact, such that its first five lines lie within the line width of the IR laser; the levels $J'' = 1f$–$5f$ can then be excited simultaneously. This reduces the time for data collection, but loses the J-selectivity of double resonance. However the line assignments could be made without difficulty by combination differences.

The structure of the 2^1B^1 polyad is similar to that of the B^1 polyad analyzed by Utz et al. [39], the main difference being that the 2^16^1 level lies 9.6 cm^{-1} above the 2^14^1 level, whereas 6^1 lies only 3.4 cm^{-1} above 4^1. This is in contrast to the 3^nB^1 polyads, where the ν_6' member always lies below the ν_4' member [10]. There is no doubt about the assignments because the branch structures are unambiguous. Seen in double resonance via the f-symmetry component of the $\nu_3 + \nu_4''$ combination level, the 2^16^1 level (b_u symmetry) gives a $K' = 0$ sub-band with R and P branches, while the $K' = 0$ sub-band of 2^14^1 (a_u symmetry) has only a Q branch.

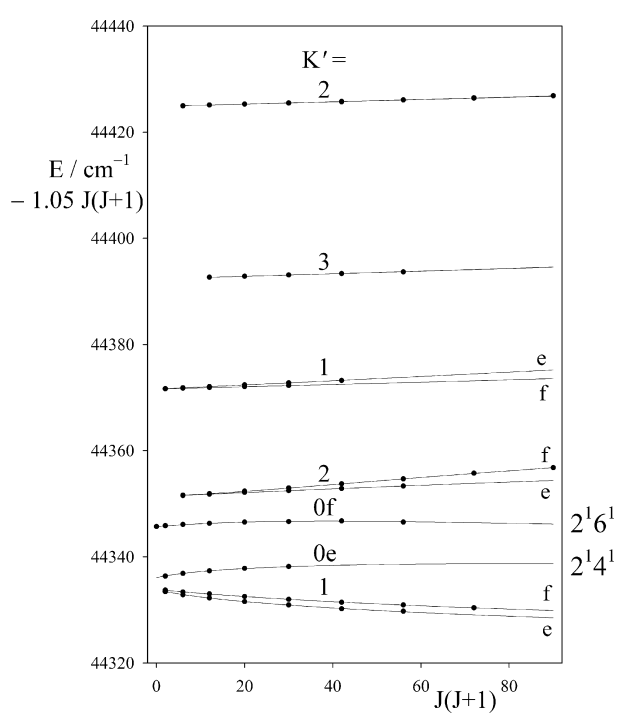

Fig. 2. Reduced term value plot of the 2^1B^1 polyad, where the upper state energy levels, less 1.05 $J(J+1)$, are plotted against $J(J+1)$. a-Axis Coriolis interaction between the two $K' = 1$ levels pushes the lower $K' = 1$ level (nominally 2^14^1) below its $K' = 0$ level; b-axis Coriolis coupling between this $K' = 1$ level and the two $K' = 0$ levels is responsible for the curvatures in the plots. Points represent observed levels; lines are calculated from the results of the final least squares fit.

Fig. 2 is a reduced energy level plot showing the assigned upper state term values together with the patterns calculated from the final least squares fit, described below. The strong b-axis Coriolis coupling between the two $K = 0$ levels and the lower $K = 1$ level is evident in the curvature of the plots for those levels. Interestingly, the largest asymmetry splitting occurs in the lower $K = 2$ level, presumably because of the proximity of the 2^16^1, $K = 0$ level. The asymmetry splittings of the two $K = 1$ levels are smaller than expected for the Ã state. In the absence of the a-axis Coriolis coupling, these two levels would have equal and opposite asymmetry splittings, each about twice as large as is found. The a-axis Coriolis coupling between them results in partial cancellation of their splittings.

The 2^1B^1 polyad lies just below the B^3 polyad and, with the strong a-axis Coriolis coupling pushing the uppermost level of each K value some distance above the others, the upper $K = 2$ stack of the 2^1B^1 polyad lies only 40 cm^{-1} below the lowest $K = 2$ stack of the B^3 polyad. Obviously there must be Fermi resonance between the polyads, but the small shifts that result can be absorbed into sets of effective parameters for them.

The seven observed K-stacks of the 2^1B^1 polyad have been fitted by least squares to the Hamiltonian of Eq. (1). The resulting parameters are given in Table 1. To allow for the Fermi resonance with the B^3 polyad, a centrifugal distortion correction to the a-axis Coriolis constant, called $D(2A\zeta^a_{46})_K$, was added to the parameter set. It reduced the r.m.s. error by about 30%. The rotational and Coriolis constants are found to be very similar to those determined by Utz et al. [39] for the B^1 polyad, though this is possibly fortuitous since there are extremely strong correlations between the two A rotational constants and the a-axis Coriolis parameters. We note that the mean of the two A constants, 12.894 cm^{-1}, is almost identical to the A constant of the 2^1 level, 12.902 cm^{-1}. With the rotational constants taken from the 2^1 level, the zeta sum rule [37],

$$(\zeta^a_{46})^2 + (\zeta^b_{46})^2 = 1, \tag{3}$$

holds very well, with the sum of the squares of the derived zeta parameters equal to 1.026. The upper state term values used in the fit are listed in the Appendix.

5.2. The interacting $2^13^1B^1$ and 3^1B^3 polyads

Low resolution spectra of the overlapping $2^13^1B^1$ and 3^1B^3 polyads taken by IR–UV double resonance via the ν_3'' fundamental showed that there are seven $K' = 1$ stacks present, although only six are expected. We have therefore gone to some length to obtain a full analysis in order to clarify the vibrational assignments. It turns out that the "extra" stack is the highest of the seven in

Table 1
Rotational and Coriolis constants from a least squares fit of the Ã, 2^1B^1 polyad. Values in cm^{-1}.

T_0 (2^14^1)	44336.08 ± 0.04	A(2^14^1)	11.411 ± 0.50
T_0 (2^16^1)	44345.69 ± 0.03	½($B + C$)	1.0750 ± 0.0027
$2A\zeta^a_{46}$	17.928 ± 0.13	B–C	0.1080 ± 0.0090
$B\zeta^b_{46}$	0.821 ± 0.009	A(2^16^1)	14.376 ± 0.50
$D(2A\zeta^a_{46})_K$	−0.0902 ± 0.045	½($B + C$)	1.0601 ± 0.0033
Δ_K	0.0060 ± 0.0027	B–C	0.0813 ± 0.0078
r.m.s. error: 0.0201 cm^{-1}			

The a-axis Coriolis coupling is defined as $2A\zeta^a_{46} + D(2A\zeta^a_{46})_K K^2$.
$\zeta^a_{46} = 0.695$, $\zeta^b_{46} = 0.737$.
The centrifugal distortion parameter Δ_K is assumed to be the same for 2^14^1 and 2^16^1.
The following correlation coefficients have absolute values above 0.95:

$A(2^14^1)/A(2^16^1)$	−0.998	$2A\zeta^a_{46}/D(2A\zeta^a_{46})_K$	0.954
$A(2^14^1)/2A\zeta^a_{46}$	0.987	$A(2^14^1)/D(2A\zeta^a_{46})_K$	0.988
$A(2^16^1)/2A\zeta^a_{46}$	−0.981	$A(2^16^1)/D(2A\zeta^a_{46})_K$	−0.994

energy, and lies 8.2 cm^{-1} above the topmost $K' = 1$ stack of 3^1B^3. There is no obvious vibrational assignment for the "extra" stack within the manifold of the S_1-*trans* ($\tilde{A}^1A_u$) state because every vibrational level expected in this energy region has been observed. Either it belongs to the S_1-*cis* state, or it belongs to a higher S_1-*trans* polyad where anharmonicity has pushed one of the component levels down by a huge amount. In either case it presumably interacts with the 3^1B^3 levels, causing an energy shift, though this is hard to quantify.

The structure of the $2^13^1B^1$ and 3^1B^3 polyads is distorted because the ν_3'/ν_6' anharmonicity has a strong effect, particularly on the 3^1B^3 polyad. Excitation of the ν_3' vibration causes the vibrational level with the largest value of ν_6' (3^16^3) to drop considerably below the rest of the polyad. The result is that the lowest energy *K*-stacks of the 3^1B^3 polyad lie in the low-*K* region of the $2^13^1B^1$ polyad. A further complication is that there is non-negligible Fermi resonance between the two polyads.

The two interacting polyads have been recorded by IR–UV double resonance, using rotational levels of the ν_3'' fundamental and $\nu_3 + \nu_4''$ combination level as intermediates, as described above for the 2^1B^1 polyad. Most of the analysis was carried out from spectra taken via the Q branch of the $\nu_3 + \nu_4''$ band, which gave the whole $J'' = 1f$–$5f$ spectrum in one recording, with consistent calibration. The line assignments could be made by combination differences, assisted for the crowded regions by spectra taken via the P(3) line of the $\nu_3 + \nu_4''$ band (populating $J'' = 2e$). Various "one-photon" bands, excited by the UV laser alone when its frequency happens to coincide with an unrelated absorption band, could be distinguished by comparing the Q- and P-pumped spectra.

Fig. 3 shows the rotational energy level structure of the two polyads, less 1.05 $J(J+1)$ cm^{-1}, plotted against $J(J+1)$. Every assigned *K*-stack is shown, except the highest $K' = 2$ stack, which lies off the top of the figure near 45712 cm^{-1}. The *K* values of the various stacks, as given by the first lines of the branches, are marked in two columns, one for the $2^13^1B^1$ polyad and the other for the 3^1B^3 polyad. The process of assigning the *K*-stacks to the polyads was complicated by the Fermi resonance and by the fact that some of the weaker sub-bands were not found until the late stages of the analysis.

Sizeable interactions occur among the levels in the central part of the structure. The most unexpected is the group of interacting $K = 1$, 3 and 4 levels near 45500 cm^{-1}. Their spectrum is shown in Fig. 4, as seen in double resonance via the Q branch of the $\nu_3 + \nu_4''$ band. None of these levels should have given bands in Fig. 4 according to the selection rule $K' - \ell'' = \pm 1$, since the intermediate level has $\ell'' = 1$. It appears that the intensity comes from the very intense $K' = 0$ bands near 45540 cm^{-1}, and is transferred to the $K' = 1$ band by *b*-axis Coriolis coupling. The rotational level pattern shows that the $K' = 3$ stack gets its intensity by a combination of *b*-axis coupling with nearby $K' = 2$ stacks and asymmetry mixing with the $K' = 1$ stack. Finally the $K' = 4$ stack interacts with the $K' = 3$ stack, again by *b*-axis coupling. Surprisingly, the $K' = 3$ stack does not appear in double resonance spectra taken via the ν_3'' fundamental ($\ell'' = 0$), although the $K' = 4$ stack gives quite strong lines. Evidently the *K* quantum number loses its meaning completely in the presence of the strong *b*-axis coupling. A similar situation was noted by Utz et al. [39] in their analysis of the B^1 polyad.

An interesting avoided crossing occurs between the $K' = 1$ and 2 stacks near 45460 cm^{-1}, illustrated in Fig. 5. In zero order the stacks belong to different polyads, and have *B* values such that they cross through each other between $J = 5$ and 6. The minimum energy separation, which represents the strength of the Fermi resonances, is 1.36 cm^{-1}. A similar perturbation occurs between the $K' = 2$ and 3 stacks near 45420 cm^{-1}; there is clearly an avoided crossing, since the intensity is progressively transferred from the

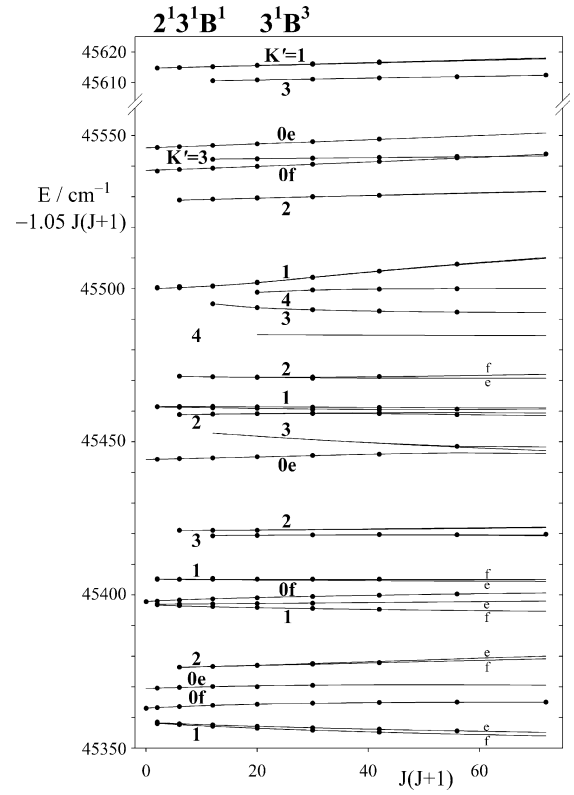

Fig. 3. Energy levels of the interacting $2^13^1B^1$ and 3^1B^3 polyads, less 1.05 $J(J+1)$, plotted against $J(J+1)$. The nominal *K* values of the rotational levels, as obtained from the first lines of the relevant branches, are indicated in two columns; left column, $2^13^1B^1$ polyad, right column, 3^1B^3 polyad. Several avoided crossings between the *K* sub-levels occur in the central part of the figure. Points are observed rotational levels, lines are calculated from the results of the final least squares fit. All the observed *K* sub-levels are shown, with the exception of the highest $K' = 2$ sub-level, which lies near 45712 cm^{-1}.

nominal $K' = 2$ stack to the nominal $K' = 3$ stack with increasing *J*, but the rotational levels diverge starting from the lowest *J* values. The lowest $K' = 3$ stack of the 3^1B^3 polyad, near 45450 cm^{-1}, could not be identified, although most of the other $K' = 3$ stacks appear weakly. However its presence is shown by the avoided crossing with the $K' = 0e$ stack immediately below, where the $J = 7$ level is out of place.

Occasionally the rotational structures of two *K*-stacks cross through each other without a noticeable perturbation occurring. An example is the crossing between the upper $K' = 3$ stack of $2^13^1B^1$ and the upper $K' = 0f$ of 3^1B^3 near 45540 cm^{-1}. There are no measurable shifts at the crossing, and calculations of the level structure show that the shifts will be less than 0.01 cm^{-1}. Another example is the crossing of the upper $K' = 0e$ and the lowest $K' = 5$ of 3^1B^3 (not shown in Fig. 3) at $J = 7$; no measurable shifts are expected.

A few of the sub-bands, such as the upper $K' = 0f$ sub-band of the 3^1B^3 polyad illustrated in Fig. 4, show evidence of perturbations by triplet states. These take the form of small splittings of the lines into two or three components spread over up to about 0.4 cm^{-1}. The lines involved were not included in the final data set.

The results of a least squares treatment are given in Table 2. The levels of the $2^13^1B^1$ polyad were modeled with rotational constants *A*, ½(*B* + *C*) and *B*–*C* for the two vibrational levels, together with Coriolis constants $2A\zeta^a_{46}$ and $B\zeta^b_{46}$. The operators for the Fermi resonances were taken as

$$H = k_{244}Q_2Q_4^2 + k_{266}Q_2Q_6^2, \quad (4)$$

which give matrix elements

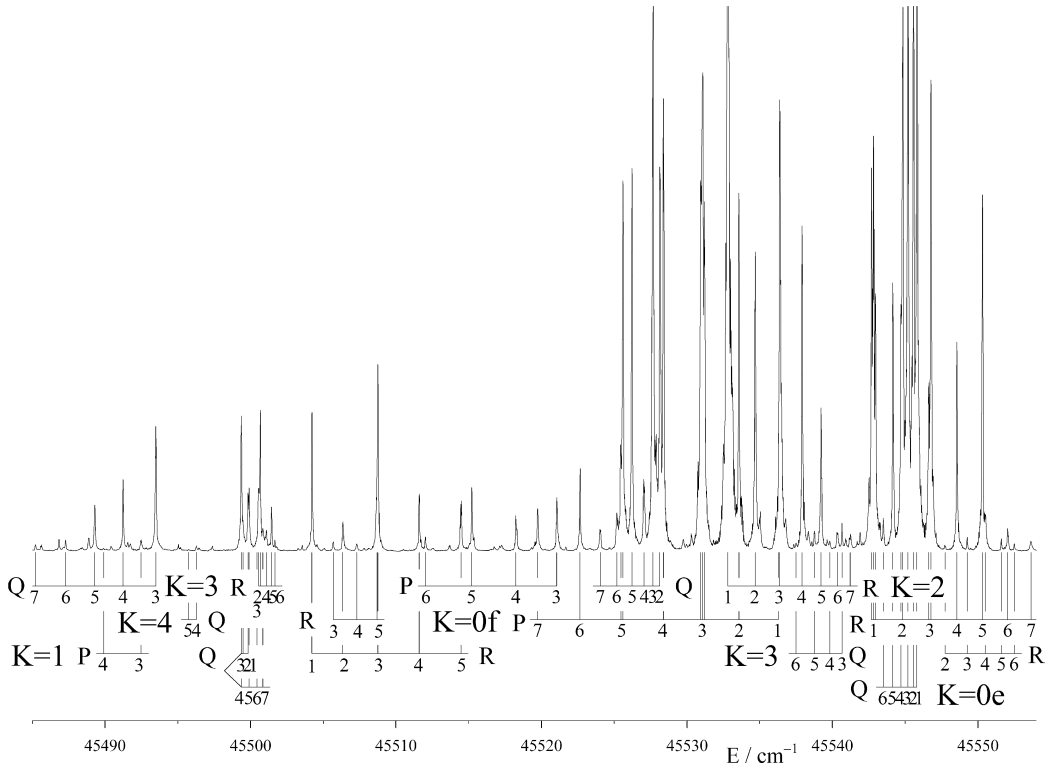

Fig. 4. The region 45485–45554 cm^{-1} in the IR–UV double resonance spectrum of acetylene, showing seven overlapping sub-bands with K' = 0–4. The IR laser was tuned to the Q branch head of the $\tilde{X}$, $\nu_3 + \nu_4''$ band ($\ell'' = 1$), populating the J'' = 1*f*–5*f* levels simultaneously. Some small splittings resulting from triplet perturbations can be seen in the K' = 0*f* sub-band.

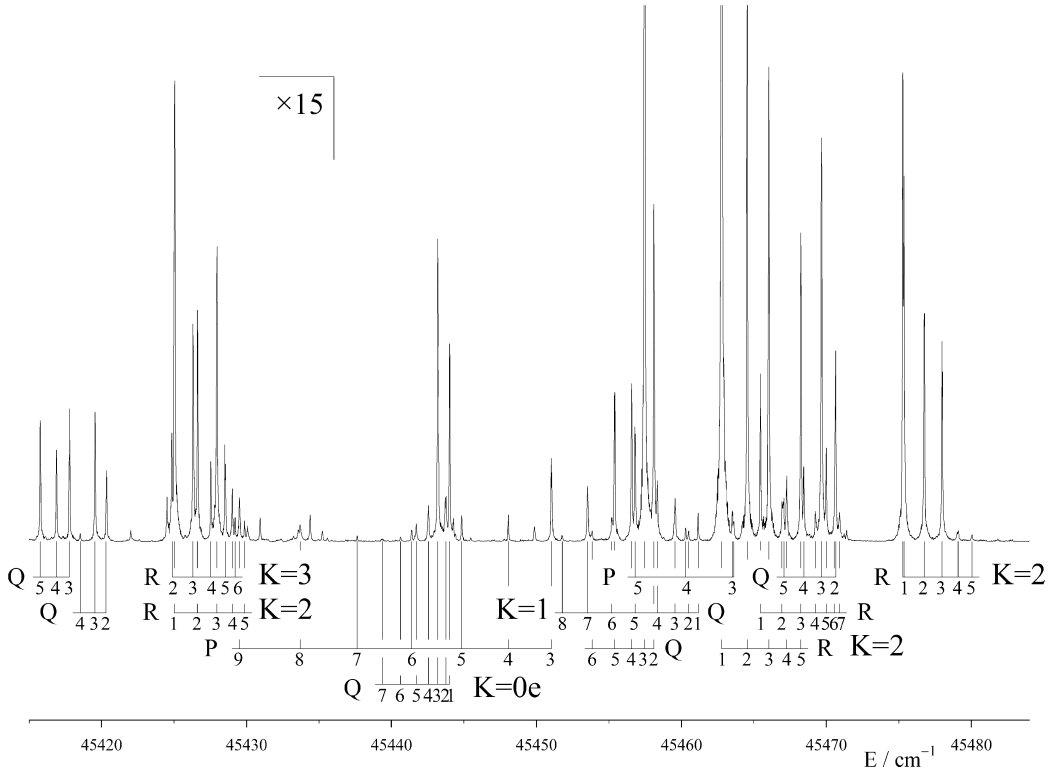

Fig. 5. The region 45415–45484 cm^{-1} in the double resonance spectrum of acetylene, showing six overlapping sub-bands. This figure is a continuation of Fig. 4 to lower frequency. Below 45436 cm^{-1} the intensity scale of the spectrum has been expanded by a factor of 15 to show the weaker sub-bands in that region.

Table 2
Rotational constants from simultaneous least squares fits of the $2^13^1B^1$ and 3^1B^3 polyads of the $\tilde{A}^1A_u$ state of acetylene. Values in cm^{-1}.

T_0 ($2^13^14^1$)	45369.82 ± 0.11	T_0 (3^14^3)	45502.16 ± 0.71
T_0 ($2^13^16^1$)	45364.12 ± 0.11	T_0 ($3^14^26^1$)	45517.43 ± 0.17
$2A^{\zeta^a}_{\varsigma 46}$ ($2^13^1B^1$)	20.971 ± 0.057	T_0 ($3^14^16^2$)	45487.64 ± 0.67
$B^{\zeta^b}_{\varsigma 46}$ ($2^13^1B^1$)	0.7644 ± 0.0108	T_0 (3^16^3)	45417.73 ± 0.23
A ($2^13^14^1$)	10.709 ± 0.228	K_{4466}	−57.865 ± 0.123
½(B + C)	1.0784 ± 0.0048	$K_{4466,DK}$	0.077 ± 0.092
B–C	0.1235 ± 0.0171	$2A^{\zeta^a}_{\varsigma 46}$ (3^1B^3)	20.596 ± 0.050
A ($2^13^16^1$)	16.796 ± 0.236	$B^{\zeta^b}_{\varsigma 46}$ (3^1B^3)	0.7788 ± 0.0084
½(B + C)	1.0545 ± 0.0036	A (3^14^3)	13.582 ± 0.321
B–C	0.0868 ± 0.0153	½(B + C)	1.0755 ± 0.0036
$D(2A^{\zeta^a}_{\varsigma 46})_K$ ($2^13^1B^1$)	−0.2701 ± 0.0393	B–C	0.0934 ± 0.0171
		A ($3^14^26^1$)	13.231 ± 0.136
k_{244}	−7.36 ± 1.14	A ($3^14^16^2$)	14.730 ± 0.322
k_{266}	8.702 ± 0.150	A (3^16^3)	14.873 ± 0.080
		½(B + C)	1.0780 ± 0.0042
		B–C	0.1532 ± 0.0180
		D $(2A^{\zeta^a}_{\varsigma 46})_K$ (3^1B^3)	−0.0589 ± 0.0075
		Δ_K (3^14^3)	0.0689 ± 0.0243
		Δ_K (3^16^3)	−0.0909 ± 0.0240
		$K_{4466,DJ}$	−0.0035 ± 0.0015
r.m.s. error: 0.0453 cm^{-1}			

Error limits are three standard deviations.
The following correlation coefficients have absolute values above 0.95:

A ($2^13^14^1$)/A ($2^13^16^1$):	0.998	A ($2^13^14^1$)/D $(2A^{\zeta^a}_{\varsigma 46})_K$ ($2^13^1B^1$):	0.994
T_0 (3^14^3)/T_0 ($3^14^16^2$):	−0.985	A ($2^13^16^1$)/D $(2A^{\zeta^a}_{\varsigma 46})_K$ ($2^13^1B^1$):	−0.991
A (3^14^3)/T_0 (3^14^3):	−0.975	A (3^14^3)/T_0 ($3^14^16^2$):	0.981
Δ_K (3^14^3)/Δ_K (3^16^3):	−0.982		

The $J' = 0$ levels of the vibrational states are calculated to lie at
e-symmetry: 45369.48 cm^{-1} ($2^13^14^1$); 45444.27 and 45545.87 cm^{-1} ($3^14^16^2$ and 3^14^3).
f-symmetry: 45362.99 cm^{-1} ($2^13^16^1$); 45397.81 and 45538.50 cm^{-1} (3^16^3 and $3^14^26^1$).
The differences between these values and those in the body of the table arise from the Fermi and Darling–Dennison resonances.

$$\begin{aligned}
\left\langle 2^13^14^1|H|3^14^3\right\rangle &= \frac{1}{2}\sqrt{3}k_{244}\\
\left\langle 2^13^14^1|H|3^14^16^2\right\rangle &= \frac{1}{2}k_{266}\\
\left\langle 2^13^16^1|H|3^16^3\right\rangle &= \frac{1}{2}\sqrt{3}k_{266}\\
\left\langle 2^13^16^1|H|3^14^26^1\right\rangle &= \frac{1}{2}k_{244}.
\end{aligned} \tag{5}$$

As explained following Eq. (2), the transformation that makes the Coriolis matrix elements real changes the signs of the k_{266} terms in Eq. (5), making them negative.

The ν'_3/ν'_6 anharmonicity complicated the fit of the 3^1B^3 polyad. It was found that the various avoided crossings in the *J*-structure could not be fitted satisfactorily until the *K*-structure was reproduced correctly, but in order to do this it was necessary to float the *A* constants for each of the four vibrational components, and introduce a number of centrifugal distortion parameters. Some of these have unreasonable values, and should be treated just as fitting parameters, without physical meaning. The Δ_K parameters are a case in point. The parameters $\Delta_K(3^14^3)$ and $\Delta_K(3^16^3)$ were fitted by least squares, with the values of the Δ_K parameters for the other two vibrational levels of the polyad interpolated between them. The final values are far larger than expected, of opposite sign and also strongly correlated. Another unreasonable value is that for the parameter $D(2A^{\zeta^a}_{\varsigma 46})_K$ of the $2^13^1B^1$ polyad. For the *J*-structure of the 3^1B^3 polyad, the parameters ½(B + C) and B–C for the 3^14^3 and 3^16^3 levels were fitted, with the values for the other vibrational levels interpolated between them.

It was sometimes difficult in the least squares treatment to match the observed and calculated energies, particularly at the avoided crossings. The procedure adopted was to sort the energy levels by their nominal *K* values, which were then placed in ascending order. At the final stages, when the pattern of the *K*-structure had been established, the levels of each *J* and *e*/*f* symmetry were indexed by their energy order. This method copes with the avoided crossings very well, but breaks down if a large change in a parameter interchanges the energy order of two *K*-stacks. In the end, 216 rotational term values from 24 *K*-stacks were fitted with 33 parameters, giving an r.m.s. error of 0.045 cm^{-1}. It is very clear that the simple model of Eq. (1) is starting to break down for these polyads. The line measurements are probably good to better than 0.03 cm^{-1} but, if no centrifugal distortion terms are included, the best fit to Eqs. (1) and (5) gives an r.m.s. error of about 0.12 cm^{-1}. Nevertheless, with the centrifugal distortion terms included, the courses of all the avoided crossings are reproduced with good accuracy. The upper state term values are listed in the Appendix.

One of the reasons for trying to get a good fit to the structure was to determine the Fermi resonance parameters, since these are important for extending the vibrational assignments to higher energy. It was found that the parameter k_{266} is quite well determined, though k_{244} is more approximate. Their absolute signs are not determinable, but their relative signs are opposite. To some extent their values must depend on the centrifugal distortion terms that were added in order to fit the *K*-structure. However, it was found that the value of k_{266} did not vary much from 8.7 cm^{-1} as these various terms were included.

As indicated at the beginning of this Section, the strong ν'_3/ν'_6 anharmonicity causes the 3^16^3 basis level of the 3^1B^3 polyad to drop a long way below the other three basis levels (see Table 2). As a result, the Darling–Dennison resonance between the 3^16^3 and $3^14^26^1$ levels causes only a modest shift of 20 cm^{-1} (as can be seen from the calculated $J = 0$ energies in Table 2). On the other hand, the 3^14^3 and $3^14^16^2$ levels, which lie quite close in zero order, interact strongly, such that the nominal 3^14^3 state ends up as the top member of the polyad, 7 cm^{-1} above the nominal $3^14^26^1$ state. These two states form an a_u/b_u pair, of the type described in Ref. [43], which demonstrates the development of vibrational angular

momentum patterns in the higher bending polyads. However the effect is not as marked when v_3' is excited, compared to the pure bending polyads, because the v_3'/v_6' anharmonicity distorts the polyad structure.

5.3. The 2^2B^1 polyad

The 2^2B^1 polyad lies immediately above the 3^1B^3 polyad which, as just described, contains an "extra" $K' = 1$ stack. Another "extra" K-stack (this time with $K' = 0$, a_u symmetry) lies at 45735 cm^{-1}, just above the predicted position of the 2^2B^1 polyad. It therefore becomes important to locate the 2^2B^1 polyad securely, in order to be sure that the "extra" stacks are not related to it. The 2^2B^1 polyad is expected to be much weaker than the 2^1B^1 polyad, since the 2_0^2 band (which was only found recently [41]) is much weaker than the 2_0^1 band. We have searched for the $K' = 0$ and 2 levels of the 2^2B^1 polyad using IR–UV double resonance. Despite the poor signal-to-noise ratio it seems that the $K' = 0$ sub-band of 2^26^1 can be definitely identified, and the upper $K' = 2$ sub-band of the polyad possibly so. There is still some doubt about the 2^24^1 level.

The lines used for the IR pumping were isolated P branch lines of the $\nu_3 + \nu_4''$ combination band. These populate the *e*-symmetry rotational levels of $\nu_3 + \nu_4''$, such that levels of the $\tilde{A}$ state with b_u vibrational symmetry give Q branches in IR–UV double resonance, and upper states with a_u symmetry give R and P branches. The 2^26^1 (b_u), $K' = 0$ sub-band, which appears as a weak Q branch at 45702.8 cm^{-1}, is within 0.1 cm^{-1} of where it is predicted, based on anharmonicity constants derived from the known positions of 2^1, 2^2 and the bending polyads B^1 and 2^1B^1. The anharmonicity constants predict the 2^24^1 (a_u), $K' = 0$ sub-band to lie at 45687 cm^{-1}. We have found nothing with the correct appearance near there, though a possible P and R branch pair lies at 45704.5 cm^{-1}, some 17 cm^{-1} higher than predicted. This region is dominated by very intense lines from the highest $K' = 2$ sub-band of the 3^1B^3 polyad, and it could be that artifacts of the blending have confused the assignments, despite the use of J''-selected double resonance. The $K' = 1$ sub-bands of the 2^2B^1 polyad are not expected to appear in double resonance via an $\ell'' = 1$ intermediate level, and have not been looked for.

A calculation of the $K' = 2$ sub-band energies, based on the predicted $K' = 0$ origins, together with rotational and Coriolis constants from the 2^1B^1 polyad, places them at 45705 and 45780 cm^{-1}. Nothing assignable as $K' = 2$ appears at the lower energy, but $K' = 2$ sub-bands are found at 45777.9 and 45790.8 cm^{-1}. It seems that the lower sub-band belongs to 2^2B^1 in zero-order, while the upper $K' = 2$ state is associated with the "extra" $K' = 0$ level at 45735 cm^{-1}. No least squares fitting has been attempted for the 2^2B^1 polyad, since only three fragmentary sub-bands have been assigned. The upper state term values are listed in the Appendix.

The ν_4' member of the various B^1 polyads is always weaker than the ν_6' member, so that it is perhaps not surprising that we could not identify the 2^24^1, $K' = 0$ sub-band securely. Nevertheless the good agreement of the position of the 2^26^1, $K' = 0$ sub-band with the prediction from the anharmonicity constants suggests that there is nothing unusual about the 2^2B^1 polyad. The "extra" K stacks at 45623 cm^{-1} ($K' = 1$) and 45735 cm^{-1} ($K' = 0$, a_u) therefore appear not to belong to the 2^2B^1 polyad.

6. Combination polyads observed in one-photon laser excitation

With the *a*-axis Coriolis coupling disrupting the asymmetric top K-structure so severely, it is not possible to get a satisfactory least squares fit to a bending polyad without data from $K' = 0$, 1 and 2 stacks. As described above, two sets of experiments are needed to provide such data for the *gerade* bending levels, because of the rotational selection rule $K' - \ell'' = \pm 1$. The $K' = 1$ levels can be recorded in jet-cooled laser excitation spectra from the ground vibrational state, where $\ell'' = 0$, but to record spectra of the $K' = 0$ and 2 levels it is necessary to warm the jet so that there is sufficient population in the ν_4'' fundamental, where $\ell'' = 1$. High sensitivity experiments with a cold jet have been carried out for the region up to 47000 cm^{-1}, though with decreasing efficiency at the highest frequencies because of predissociation. Experiments with a warmed jet have so far not been attempted beyond 46000 cm^{-1}.

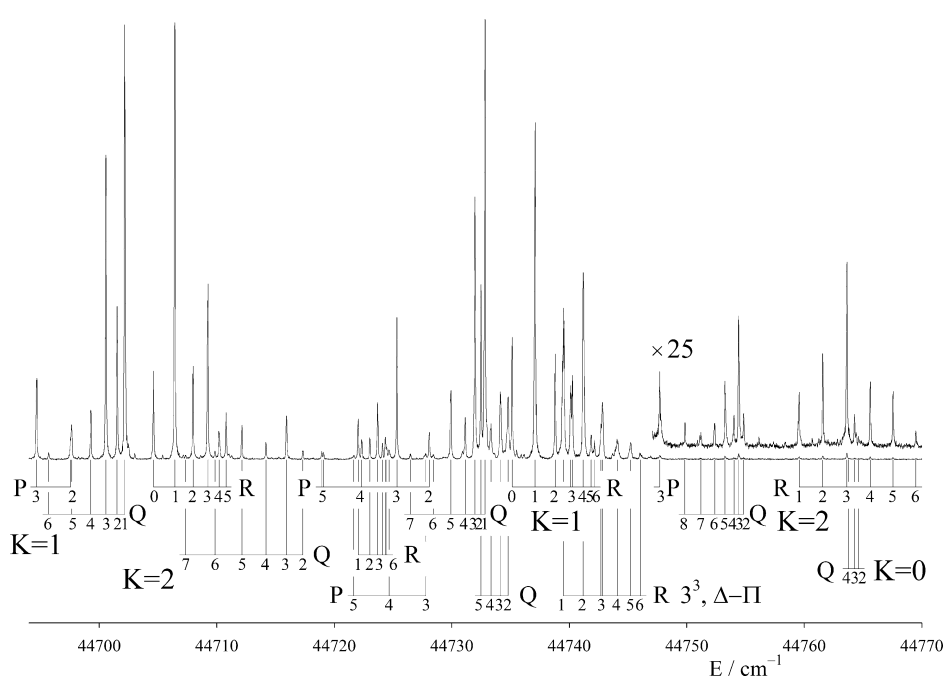

Fig. 6. Low frequency part of the 3^1B^2 polyad of acetylene, as seen in jet-cooled laser excitation from the ground vibrational level. The comparatively intense, and very strongly red-degraded $K = 2$–0 sub-band near 44719 cm^{-1} gets its intensity by *b*-axis Coriolis coupling with the $K = 1$–0 sub-band near 44733 cm^{-1}. The intensity scale of the spectrum has been expanded by a factor of 25 at the high frequency end in order to show the weak Coriolis-induced $K = 2$–0 and 0–0 sub-bands near 44760 cm^{-1}.

6.1. The 3^1B^2 polyad

The 3^1B^2 polyad, near 44700 cm^{-1}, has the simplest spectrum of all of the B^2-type polyads observed in one-photon LIF. It lies at sufficiently low energy that it does not suffer from overlap with other polyads, while the anharmonicity between modes 3 and 6 causes the lowest member of the polyad (nominally 3^16^2) to drop well below the other members. Compared to the B^2 polyad, the anharmonicity greatly reduces the damaging effect of the *b*-axis Coriolis resonance on the qualitative appearance of the spectrum. All three $K' = 1$ bands are readily recognizable and sufficiently free from overlap with other bands to allow straightforward rotational analyses. The low frequency part of the polyad, as seen in laser excitation from the ground level, is illustrated in Fig. 6. The lowest two $K' = 1$ bands lie between the intense 3^34_1, Σ–Π and Δ–Π hot bands.

There is in fact a systematic coincidence between the strong hot bands of the type 3^n4_1 and weaker cold bands going to the $3^{n-2}B^2$ polyads. This can cause confusion when low resolution spectra are examined. For example, in the survey spectra of Ref. [42] there are bands with barely detectable intensity close to the expected positions for B^2 and 3^1B^2. Upon closer inspection, despite the low temperature of the free-jet expansion, the positions of these bands are found to match those of the known 3^n4_1 hot bands and do not correspond to polyads formed from the low-frequency bending modes.

There are no low-*J* avoided crossings between the *K* stacks of the 3^1B^2 polyad members, but the *b*-axis Coriolis resonance is sufficiently strong that, despite the rotational selection rule $K' - \ell'' = \pm 1$, seven of the nine $K' = 0$–2 levels of the polyad appear in the cold jet spectrum; the exceptions are the middle $K' = 0$ level, which has b_g symmetry, and the highest $K' = 2$ level, which is expected to lie 85 cm^{-1} above the highest $K' = 1$. As a result of the *a*-axis Coriolis interactions, the lowest vibrational level of the polyad has very compressed *K*-structure, with its $K' = 2$ sublevel only 16 cm^{-1} above its $K' = 1$. The $K' = 2$ sub-level is strongly affected by *b*-axis Coriolis resonance with the second $K' = 1$, so that the R branch going to it (near 44722 cm^{-1}) appears very compact in the spectrum. As Fig. 6 shows, the R(1)–R(6) lines fall within a span of only 2.5 cm^{-1}.

The middle $K' = 2$ sub-band and the uppermost $K' = 0$ sub-band appear in Fig. 6 as a result of the Coriolis interactions. Spectra recorded in a warmed beam confirm their assignments, but do not give evidence for any new sub-bands. The sub-band terminating on the highest $K' = 2$ level is predicted to lie hidden under the very intense 3^2_0, $K' = 1$ cold band, and has not been searched for.

The observed rotational term values of the seven observed *K*-stacks have been fitted to a Hamiltonian of the same form as that used for the B^2 polyad. The results of the fit are given in Table 3. Despite the lowering of the 3^16^2 level by the ν'_3/ν'_6 anharmonicity, no additional centrifugal distortion parameters were required to fit the data to within the measurement uncertainty. Comparing the parameters for 3^1B^2 and B^2, the most significant difference is the 10% increase in the parameters K_{4466} and $2A\zeta^a$ on excitation of ν'_3.

Table 3
Rotational and Coriolis constants from a least squares fit of the Ã, 3^1B^2 polyad. Values in cm^{-1}.

T_0 (3^16^2)	44708.96 ± 0.13	A (3^16^2)	14.238 ± 0.073
T_0 (3^14^2)	44748.83 ± 0.13	½($B + C$)	1.0757 ± 0.0012
T_0 ($3^14^16^1$)	44749.61 ± 0.03	B–C	0.1153 ± 0.0026
$2A\zeta^a_{46}$	20.625 ± 0.017	A (3^14^2)	14.055 ± 0.069
$B\zeta^b_{46}$	0.784 ± 0.005	½($B + C$)	1.0772 ± 0.0010
K_{4466}	−60.101 ± 0.166	B–C	0.1070 ± 0.0029
r.m.s. error: 0.032 cm^{-1}			

The $J' = K' = 0$ levels are calculated to lie at 44692.84 (3^16^2), 44749.61 ($3^14^16^1$) and 44764.96 (3^14^2) cm^{-1}.

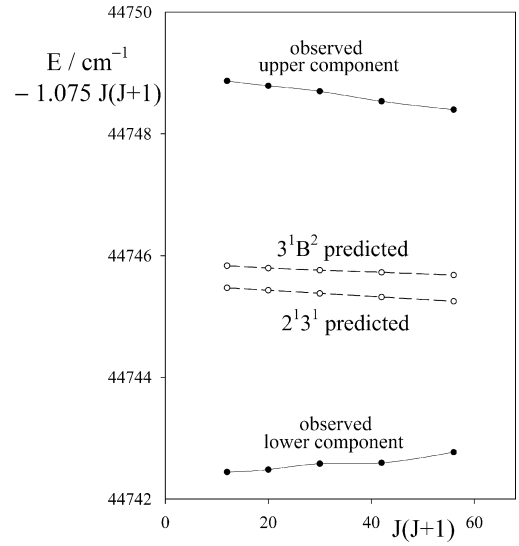

Fig. 7. Observed and predicted rotational level structure at the perturbation between the $K' = 3$ stacks of the 2^13^1 and 3^1B^2 polyads, plotted against $J(J + 1)$. The predicted zero-order level positions, as obtained from least squares fits to lower-*K* stacks, are shown in the centre of the figure; the observed levels (from measurements communicated to us by Dr. J.K.G. Watson) are shown at the top and bottom of the figure.

The $B\zeta$ parameter undergoes a corresponding, but smaller percentage decrease. Although the addition of one quantum of ν'_3 restores some of the regularity of the observed spectrum, it only slightly reduces the degree of mixing of the 3^14^2 and 3^16^2 normal mode basis states in the final vibrational eigenstates. The reason for this is that the anharmonic shifts that separate the zero-order states are mostly offset by the larger value of the Darling–Dennison parameter, K_{4466}.

After the measured $K' = 0$–2 stacks had been fitted, it was noticed that the lowest $K' = 3$ sublevel of 3^1B^2 was predicted to lie at almost exactly the same energy as the $K' = 3$ sublevel of 2^13^1, which had been reported as perturbed by Watson et al. [37] The near-degeneracy is quite striking: the predicted values given by Watson et al. for 2^13^1 $K' = 3$, based on fitting the unperturbed $K' = 0$–2 sublevels, coincide with the predictions of our model for the $K' = 3$ sublevel of 3^1B^2 to better than 0.5 cm^{-1}. On this basis, we can now assign the lowest $K' = 3$ sublevel of 3^1B^2 as the perturbing partner to 2^13^1 $K' = 3$. Watson et al. [37] noted that this perturbation was the lowest energy perturbation that they found in the Ã state

A reduced term value plot for the perturbed levels is given in Fig. 7. The predicted term values of 3^1B^2 and 2^13^1 are shown, together with term values derived from measured line positions that were communicated privately to us by Dr. J.K.G. Watson. The observed components of the doubled band lie approximately 6.4 cm^{-1} apart and are symmetrically distributed around the predicted zero-order positions, indicating a coupling matrix element of about 3.2 cm^{-1}. An independent estimate of this value can be obtained from the anharmonic parameters k_{244} and k_{266} derived from the interacting $2^13^1B^1/3^1B^3$ polyads (see Table 2). The eigenfunction of the lowest $J' = K' = 3$ state, considering just the Darling–Dennison and *a*-axis Coriolis interactions, and allowing for the phase factor for the v_6 levels, is

$$|3^1B^2, K = 3, I\rangle = 0.62|3^14^2\rangle + 0.70i|3^14^16^1\rangle - 0.35|3^16^2\rangle. \quad (6)$$

The Fermi resonance matrix element has only two terms, by symmetry:

$$\left\langle 2^13^1|H|3^1B^2, K = 3, I\right\rangle = 0.62\left\langle 2^13^1|H|3^14^2\right\rangle - 0.35\left\langle 2^13^1|H|3^16^2\right\rangle, \quad (7)$$

where the two integrals on the right hand side are ½ k_{244} and ½ k_{266}, respectively. Taking k_{244} = 7.36 and k_{266} = 8.70 cm^{-1} from Table 2, we obtain

$$\left\langle 2^1 3^1 | H | 3^1 B^2,\ K = 3, I \right\rangle = -3.8\ \text{cm}^{-1}. \tag{8}$$

Total agreement is not expected, in view of the uncertainties in the determination of the k_{244} and k_{266} parameters, but the agreement with the (unsigned) value of 3.2 cm^{-1} from Fig. 7 seems very reasonable. The fact that the observed matrix element is small compared to k_{244} and k_{266} themselves is explained by the large amount of $|3^1 4^1 6^1\rangle$ character in the eigenfunction of Eq. (6), which does not contribute to the Fermi resonance matrix element.

A further perturbation in a single rotational level should be noted here. The J' = 2e level of the highest K' = 1 member of the 3^1B^2 polyad exhibits quantum beats with nearly 100% modulation and a beat frequency of approximately 5 MHz. The large modulation depth combined with a slow beat frequency implies a weak interaction of <0.002 cm^{-1}. It is not surprising then, that the adjacent lines in the band appear to be unaffected by the perturbation and exhibit regular fluorescence decays. In hindsight we note that the R(1) line of this sub-band is very slightly asymmetrical, but this would not have been noticed without the quantum beat information. The perturbing state is presumably a member of the triplet manifold.

6.2. The 3^2B^2 polyad

The spectrum of the 3^2B^2 polyad is centered near 45700 cm^{-1}, a region dominated by intense bands terminating on the $2^1 3^2$ vibrational level. The 3^2B^2 polyad bands are themselves significantly more intense than the other B^2-type polyads described in this work, a fact that is consistent with the observed trend of increasing intensity with higher excitation in the Franck–Condon active *trans*-bending mode, ν_3'. As a result, bands terminating on two of the three K' = 1 levels of the polyad can be seen in the survey spectrum of Ref. [42], where the upper state of the band at 45811 cm^{-1} is labeled as $3^2 4^2$.

The 3^2B^2 bands look quite similar to those of the 3^1B^2 polyad described above. There are no low-J avoided crossings between the polyad members, so the rotational assignments of the states are not complicated by b-axis Coriolis interactions. The most obvious feature is the relatively intense 45811 cm^{-1} band, which goes to the highest K' = 1 level. The sub-band terminating on the middle K' = 1 level, at 45726.12 cm^{-1}, is nearly coincident with a hot band at 45726.93 cm^{-1} terminating on 3^4 K' = 2, but is easily recognized from its intensity and the contrast between its fluorescence lifetime and that of the overlapping band. Coriolis-induced bands going to the middle K' = 2 and the highest K' = 0 levels lie in the clear and are readily recognized. The lowest K' = 0 sublevel of the 3^2B^2 polyad was located using spectra recorded with a warmed beam. Despite severe blending, the K = 0–1 sub-band was found to lie near 45032 cm^{-1}, in the tail of the K = 0–1 hot band of $2^1 3^2$.

The lowest energy K' = 1 member of the polyad, at 45653.24 cm^{-1}, was significantly more challenging to identify because of overlap by no less than four other sub-bands. These four are the tail of the intense $2^1 3^2$, K' = 1 sub-band, its accompanying K' = 0 axis-switching band, the analogous K' = 1 transition of $H^{13}C^{12}CH$ and the $3^4 4_1$, K = 0–1 hot band. The bands are illustrated in Fig. 8. Once the lines of these four bands are accounted for, only a few strong isolated lines remain, in particular the series at 45655.31, 45657.20 and 45658.83 cm^{-1}. Since no clear combination differences could be found to number these lines, stimulated emission pumping spectra (SEP) were recorded using their upper states as the intermediate levels. Specifically, spectra were recorded to the $[N''_{\text{resonance}} = 13,\ N''_{\text{stretch}} = 1]_g$ polyad of the ground state, which lies near 8300 cm^{-1} [46]. This region was chosen because it was known that the 45811 cm^{-1} level emits strongly to this polyad, and it was assumed that the other 3^2B^2 levels should do so as well, though not necessarily to the same vibrational components.

Because the vibration–rotation structure of the electronic ground state of acetylene is well understood, the patterns in SEP spectra [47] can be used to label the rotational level of the Ã state used as an intermediate. In particular, in the absence of

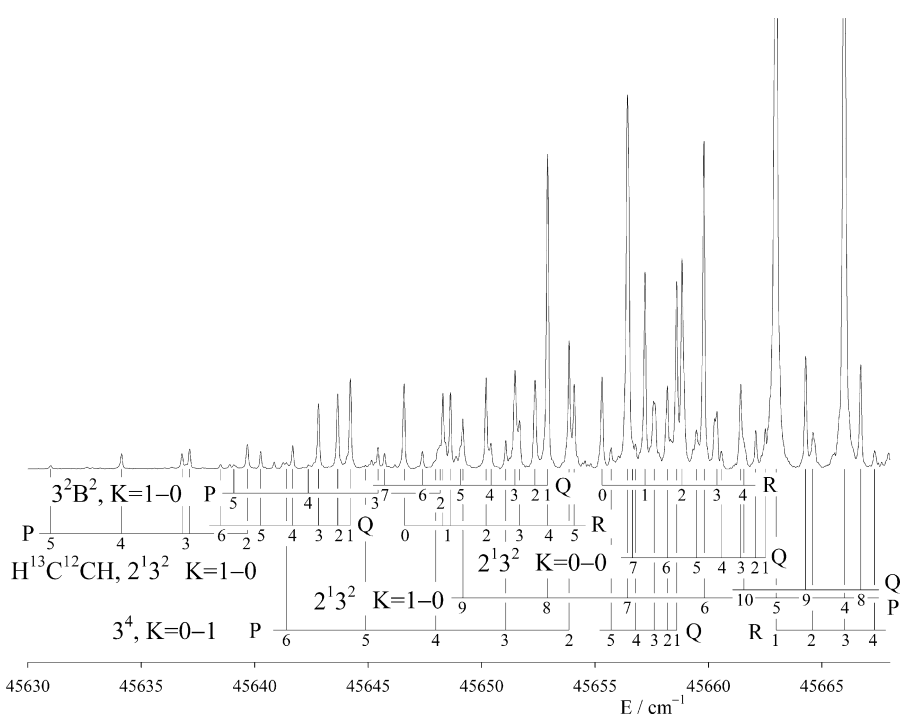

Fig. 8. The lowest 3^2B^2, K' = 1 sub-band of acetylene, overlapped by four other sub-bands. The strong structure is the tail of the $2_0^1 3_0^2$, K = 1–0 sub-band; weaker lines belong to the $H^{13}C^{12}CH$ isotopologue, the $2_0^1 3_0^2$, K = 0–0 axis-switching sub-band, and a hot band terminating on 3^4.

Table 4
Rotational and Coriolis constants from a least squares fit of the Ã, 3^2B^2 polyad. Values in cm^{-1}.

T_0 (3^26^2)	45653.95 ± 0.40	A (3^26^2)	16.178 ± 0.208
T_0 (3^24^2)	45756.86 ± 0.40	½($B + C$)	1.0808 ± 0.0021
T_0 ($3^24^16^1$)	45736.07 ± 0.02	B–C	0.1080 ± 0.0043
$2A^{\zeta^a}_{46}$	23.559 ± 0.112	A (3^24^2)	14.611 ± 0.212
$B^{\zeta^b}_{46}$	0.808 ± 0.014	½($B + C$)	1.0727 ± 0.0012
K_{4466}	−66.502 ± 0.122	B–C	0.0989 ± 0.0027
r.m.s. error: 0.024 cm^{-1}			

The $J' = K' = 0$ levels are calculated to lie at 45644.14 (3^26^2), 45736.07 ($3^24^16^1$) and 45766.67 (3^24^2) cm^{-1}.

axis-switching or accidental coincidences, the SEP spectrum via a $J' > 2$ R-branch PUMP transition contains 5 lines terminating on rotational levels of the $\Sigma_g^+(\ell'' = 0)$ and Δ_g ($\ell'' = 2$) components of every ground state vibrational level to which transitions are allowed. Q-branch PUMP transitions ($J' > 2$) give rise to 4 lines in the SEP spectrum. At lower values of J', there are fewer lines because of the restriction $J'' \geqslant \ell''$. In all cases, the upper-state assignment follows from the final-state combination differences observed in the spectrum. The three isolated lines in the LIF spectrum described above could be identified as R(0–2) since their SEP spectra contain intervals of approximately $6B''$, $10B''$, and $14B''$, where B'' is the rotational constant for the ground vibrational level of C_2H_2. Once the R branch of the 45653 cm^{-1} band had been recognized, the P and Q lines could be picked out, though in many cases they are severely blended. In particular the Q(1) line, at 45652.91 cm^{-1}, coincides with the P(8) line of the strong 2^13^2 $K' = 1$ band. The assignment of Q(1) has been confirmed by recording an SEP spectrum using it as a PUMP transition.

The six observed sublevels of the 3^2B^2 polyad (of the nine with $K = 0$–2) have been fitted to the Hamiltonian given in Eq. (1). The results of the fit are given in Table 4. Addition of a second quantum of ν_3' continues the trend noted in the 3^1B^2 polyad: the Darling–Dennison and a-axis Coriolis coupling parameters increase yet further, while the b-axis coupling is slightly reduced. The increase in the Darling–Dennison parameter is more than offset by the increased separation of the 3^24^2 and 3^26^2 basis states as a result of anharmonicity, so that the mixing of the basis states by the Darling–Dennison resonance is actually less than it is in the B^2 polyad. To be exact, the $J' = K' = 0$ eigenstates receive over 90% of their character from a single basis state. The fit model indicates only slightly more mixing for the lowest $J' = K' = 1$ eigenstate, though the upper two states form a very strongly Coriolis-coupled a_g/b_g pair.

A further advantage of SEP spectra is that they give the distribution of b_g vibrational character among the polyad members. Since a_g and b_g correlate, respectively, with the Σ_g^+ and Σ_g^- representations of $D_{\infty h}$, the Franck–Condon-allowed levels of the Ã state, with a_g vibrational symmetry, will emit to $\ell'' = 0$ states with Σ_g^+ (e) symmetry, while levels with b_g vibrational symmetry will emit to $\ell'' = 0$ states with Σ_g^- (f) symmetry. Since the e/f symmetry is reversed in Σ_g^- states, compared to Σ_g^+ states, the pattern of emission lines in transitions to them is also reversed: for $J' > 2$, Q-branch pumping gives a five-line pattern and R-branch pumping a four-line pattern. It is therefore simple to identify Σ_g^- vibrational levels in SEP spectra, and thereby assess the amount of b_g character in a given vibrational level of the Ã state.

SEP spectra have been recorded via the $J' = 1f$ (Q(1)-pumped) levels of the three $K' = 1$ stacks of the 3^2B^2 polyad. In all three SEP spectra, a feature is observed near an internal energy of 8320 cm^{-1}, terminating on what is believed to be a $J'' = 2$, $\ell'' = 2$ state. Just above this transition, but only in the spectra from the two highest energy $K' = 1$ intermediate levels, are two lines separated by approximately $6B''$. The final states of these transitions are assigned as $J'' = 0$ and 2 of a Σ_g^- vibrational level with an energy of 8322.3 cm^{-1}. To our knowledge, this state has not previously been observed, though the predictions of the multiresonant polyad Hamiltonian place a Σ_g^- member of the [13,1] polyad at 8322.5 cm^{-1} [46], in excellent agreement with our observation. The lack of intensity into this final state from the lowest $K' = 1$ polyad member is consistent with our model, which predicts <10% b_g character in this sublevel. In general, levels of the Ã state with dominant b_g vibrational character could prove useful in SEP experiments for identifying further Σ_g^- vibrational levels of the

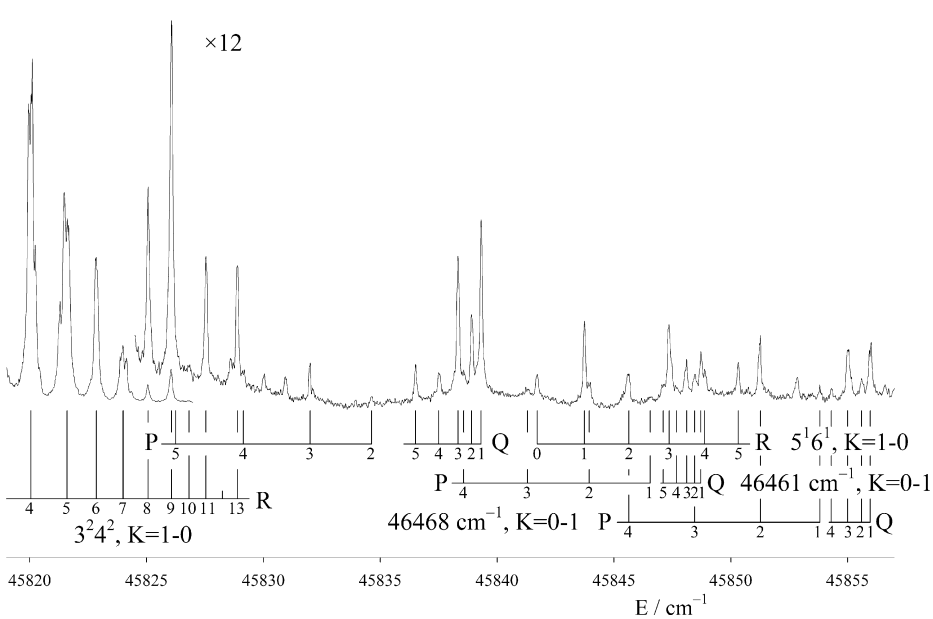

Fig. 9. LIF spectrum of jet-cooled acetylene in the region of 45819–45857 cm^{-1}. At the low frequency (left) side are the higher-J R lines of the 3^24^2 band (45811 cm^{-1}), showing structure resulting from perturbations by triplet states. The central part of the spectrum contains the 5^16^1, $K' = 1$ sub-band, and the two sub-bands at the high frequency side are $K = 0$–1 hot bands going to the interacting 2^2B^2 and 1^12^1, $K' = 0$ levels; these hot bands are labeled by the energies of their upper states (46461 and 46468 cm^{-1}).

ground state, which are presently undersampled relative to the other symmetry species.

A final note on this polyad is that many of the lines in the highest $K' = 1$ sub-band (45811 cm^{-1}) appear to be significantly broadened and structured, presumably because of interactions with the manifold of low-lying triplet states. While all lines are affected to some degree, the broadening is particularly severe for $J' = 5$–8, with the FWHM of the observed linewidth increasing to over 0.3 cm^{-1} at $J' = 6$, compared to the width of 0.06 cm^{-1} in the narrowest lines observed in our study. The splittings in the higher-J R lines of this band are illustrated in Fig. 9.

6.3. The 3^3B^2 polyad

The 3^3B^2 polyad lies above the onset of predissociation, and experiments with a warmed jet have not so far been carried out in this region. However spectra taken with a cold jet have allowed assignment of the upper two $K' = 1$ sub-bands for this polyad. As in the 3^1B^2 and 3^2B^2 polyads, the lowest $K' = 1$ sub-band is weaker than the other two, and has not been identified yet. Bands from three other polyads, 1^1B^2, 2^1B^4 and B^6, are expected in the same region, making vibrational assignments challenging.

The highest energy $K' = 1$ sub-band, at 46794.29 cm^{-1}, was already recognized in Ref. [42]. It is a fairly strong band which continues the obvious 3^n4^2 progression found in the 3^1B^2 and 3^2B^2 polyads. Because it lies so far above the other $K' = 1$ stacks of its polyad, the asymmetry splitting of the upper state is only minimally affected by the a-axis Coriolis coupling, and its magnitude (B–C = 0.074 cm^{-1}) is not much reduced from that of the zero-point level. Another, rather weaker, $K' = 1$ sub-band (as yet unassigned vibrationally) lies just below it, at 46790.74 cm^{-1}. No local interactions between the two upper states occur in the observable range of J values, though an avoided crossing between the f-symmetry components is predicted to occur at much higher J. In contrast to the 45811 cm^{-1} band, discussed in the previous Section, the 46794 cm^{-1} band does not appear to be strongly affected by triplet perturbations.

The middle $K' = 1$ sub-band, at 46692 cm^{-1}, lies 5 cm^{-1} above the 2^13^3, $K' = 1$ sub-band, and appears to have caused some confusion in the rotational assignment of the latter [38]. With the advantage of jet-cooling it is possible to recognize that two bands are present, though their branches overlap severely. The reduced upper state energies are shown plotted against $J(J + 1)$ in Fig. 10. It is clear from this figure that the senses of the asymmetry splitting are opposite in the two levels. This is as expected, since the 3^3B^2 level in question is the middle component of its polyad. The largest contributor to its wavefunction is the $3^34^16^1$ basis state, which has b_g vibrational symmetry; the sense of its splitting is therefore opposite to that of the 2^13^3 level, which has a_g symmetry. The figure shows that, in contrast to the analysis of Ref. [38], the asymmetry splitting of the 2^13^3, $K' = 1$ level is quite small at low J. Blending has made some of the measurements for the $3^34^16^1$ levels less certain, but it appears that the $K'_c = J' - 1$ (e-symmetry) components of the two vibrational levels undergo an avoided crossing at about $J = 5$, with an interaction matrix element of

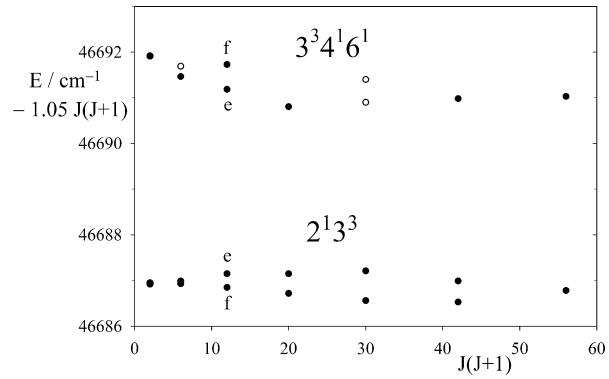

Fig. 10. Rotational energies of the interacting 2^13^3 and $3^34^16^1$, $K' = 1$ levels, less 1.05 $J(J + 1)$, plotted against $J(J + 1)$. The levels of e-symmetry undergo an avoided crossing near $J' = 5$. Open circles represent data points from blended lines.

roughly 1.6 cm^{-1}, while the separation of the $K'_c = J'$ (f-symmetry) components changes only slightly with J. The size of the interaction matrix element is consistent with the energies of the K-stacks of the 2^13^3 level given in Table XI of Ref. [38], where it can be seen that the $K' = 1$ level is about 1 cm^{-1} lower than would be expected from the energies of the $K' = 0$ and 2 stacks because they will be more detuned from resonance.

If there were no a-axis Coriolis coupling in the 3^3B^2 polyad, there would be no perturbation, since the 2^13^3 level has a_g vibrational symmetry and the $3^34^16^1$ level has b_g symmetry. However the Coriolis coupling mixes 3^34^2 and 3^36^2 character into the nominal $3^34^16^1$ level for $K' \neq 0$, which then allows the Fermi resonance operators of Eq. (4) to cause local perturbations. Since the K-structure of the 3^3B^2 polyad is very different from that of the 2^13^3 level, the other K-stacks of 2^13^3 will be less affected.

Rotational constants from a band-by-band fit to the $K' = 1$ sub-band at 46795 cm^{-1} are listed in Table 5, and the upper state term values are given in the Appendix.

6.4. The 2^1B^2 and 2^2B^2 polyads

The 2^1B^2 and 2^2B^2 polyads were discussed briefly by Steeves et al. [41] The 2^1B^2 polyad is of interest because the ν'_1 fundamental lies near its center, and causes perturbations as a result of anharmonic resonance. The rotational structure is unusually complicated because the $K' = 1$ stack of the ν'_1 fundamental happens to lie exactly where the middle $K' = 1$ and the lowest $K' = 2$ stacks of 2^1B^2 are involved in a very strong b-axis Coriolis resonance so that, with the two resonances competing, the resulting level pattern is very disorganized. We could only assign this region with the help of population labeling, where an IR laser was used to deplete the population of a selected rotational level of the ground state, modulating the fluorescence excited by the UV laser for those lines coming from the selected level. Analysis of the hot bands showed that further small perturbations occur between the $K' = 0$ stack of ν'_1 and the lowest $K' = 1$ stack of 2^1B^2, but that the $K' = 2$ stack of

Table 5
Rotational constants from band-by-band fits to miscellaneous levels of the $\tilde{A}^1A_u$ state of acetylene. Values in cm^{-1}.

T_0	3σ	½($B + C$)	B–C	rms
5^16^1, $K' = 1$	45839.519 ± 0.018	1.0867 ± 0.0014	0.0426 ± 0.0014	0.014
$2^2B^2/1^12^1$ $K' = 0$, (I)[a]	46460.58 ± 0.04	1.1112 ± 0.0016		0.076
$2^2B^2/1^12^1$ $K' = 0$, (II)[a]	46467.826 ± 0.016	1.0843 ± 0.0010		0.027
2^2B^2, $K' = 1$, III	46505.464 ± 0.019	1.0757 ± 0.0011	0.0275 ± 0.0011	0.016
3^3B^2, $K' = 1$, III	46794.29 ± 0.03	1.0869 ± 0.0041	0.074 ± 0.006	0.026

[a] These two levels arise from anharmonic interaction between the upper $K' = 0$ level of 2^2B^2 and $K' = 0$ of 1^12^1; the mixing is almost 50–50.

ν_1' lies about 10 cm^{-1} above the middle $K' = 2$ stack of 2^1B^2, and is not locally perturbed. An energy level diagram and the results of least squares fitting are given in Ref. [41].

The 2^2B^2 polyad is weaker than the 2^1B^2 polyad, and only two of its sub-bands can be securely identified. These are the highest and lowest $K' = 1$ sub-bands, at 46505.46 and 46419.04 cm^{-1}. It is clear that the 46419 cm^{-1} level undergoes strong Coriolis interactions with unseen $K = 0$ and 2 levels because it has an unusually low B value, and its asymmetry splitting is highly irregular, reversing its sense at $J = 6$. Some unusual structure near 45850 cm^{-1} had prompted us to carry out experiments with a warmed beam in that region, and led to the assignment of two $K' = 0$–1 hot bands, with upper states at 46460.58 and 46467.83 cm^{-1}. The Q and P branches of these hot bands are illustrated in Fig. 9. As explained in our earlier paper [41], these result from anharmonic resonance between the highest $K' = 0$ stack of 2^2B^2 and the $K' = 0$ stack of 1^12^1. The $K' = 1$ and 2 stacks of 1^12^1 appear to be unperturbed, and a least squares fit to them alone predicts that the 1^12^1, $K' = 0$ stack should lie at 46463.48 cm^{-1}. This would place the highest $K' = 0$ stack of 2^2B^2 at 46464.93 cm^{-1} in zero order, with an interaction matrix element of 3.6 cm^{-1}.

A global least squares fit to the 2^2B^2 polyad has been attempted, but with only three K stacks observed, one of which is involved in an anharmonic resonance, it is of limited value. Somewhat surprisingly though, the fit is very good ($\sigma = 0.011$ cm^{-1}), and reproduces the unusual asymmetry splitting of the 46419 cm^{-1} level faithfully. The position predicted by the fit for the middle $K' = 1$ sub-band coincides with the highest $K' = 1$ sub-band of the 3^1B^4 polyad, at 46434.37 cm^{-1}. This is quite a strong band, but there are not enough unassigned lines remaining to allow clear assignments of the 2^2B^2 branches. Rotational constants from a band-by-band fit to the uppermost $K' = 1$ level (46505 cm^{-1}) are given in Table 5, and the upper state term values are listed in the Appendix. Interestingly, it is not possible to give sensible rotational constants for the lower $K' = 1$ stack from a band-by-band fit because Coriolis couplings with unseen levels affect the asymmetry splitting so strongly.

6.5. The $2^13^1B^2$ and 3^1B^4 polyads

The $2^13^1B^2$ and 3^1B^4 polyads, together with the 1^13^1 level, form a complex of nine interacting vibrational levels, of which the lowest K-stacks lie near 46060 cm^{-1}. Fermi resonance is expected between the $2^13^1B^2$ and 3^1B^4 polyads, and perturbations are expected between the 1^13^1 level and the $2^13^1B^2$ polyad, in similar fashion to the perturbations between the ν_1' fundamental and the 2^1B^2 polyad. As it turns out, the K-stacks of the 1^13^1 level mostly fall in gaps in the K-structure of the $2^13^1B^2$ polyad, so that the effect of the anharmonic resonances is quite small and can be absorbed into effective constants for the levels involved. An analysis of the 1^13^1 band was given in Ref. [42]. A number of small perturbations were found in the 1^13^1 level, but none of them can be attributed to the $2^13^1B^2$ polyad.

Although only nine vibrational levels are expected in this energy region, 10 $K' = 1$ stacks are found, showing that an "extra" level, of the type discussed in Sections 5.2 and 5.3, is present. It is important to establish the detailed K-structures of these polyads so that the "extra" level can be identified securely. However this is more difficult in one-photon spectra than it is in double resonance spectra. The $K' = 1$ levels are usually easy to find because they appear in excitation spectra from the ground level. The $K' = 0$ and 2 levels require warmed jet spectra, which are more capricious experimentally, and lack the selectivity of double resonance spectra. As a result, the weaker $K' = 0$ and 2 sub-bands are not always seen, so that there can be some uncertainty in identifying what is actually observed. Careful predictions of the K-structure are needed, basing them soundly on the levels observed at lower energy.

Comparison of the 2^1B^1 and B^1 polyads shows that the anharmonicity parameters x_{24}' and x_{26}' are quite similar. Also x_{23}' is only −0.24 cm^{-1} [41]. It should therefore be possible to predict the structure of the $2^13^1B^2$ polyad to within a few cm^{-1} by adding the observed differences between corresponding levels of the 2^1B^2 and B^2 polyads to the observed energies of the 3^1B^2 polyad. This procedure assumes that x_{23}' is zero, and ignores the small shifts of up to about 3 cm^{-1} in the 2^1B^2 structure caused by the 1^1 level, but otherwise follows the usual Dunham expressions for the vibrational energies.

Because of the ν_3'/ν_6' anharmonicity, the structure of the 3^1B^4 polyad cannot be predicted in similar fashion by adding the ν_3' interval to the energies of the B^4 polyad. (In any case only eight of the 15 stacks in the B^4 polyad with $K' = 0$–2 have been located [43].) Instead, a calculation based on Eq. (1) is needed, with the zero-order vibrational energies extrapolated from anharmonicity constants derived from the 3^1B^n polyads, where $n = 0$–3. The Fermi resonance between the $2^13^1B^2$ and 3^1B^4 polyads will make small random corrections to the energies, but is probably not important for the predictions since there appear to be no pathological near-degeneracies between levels of the two polyads, of the type seen in Fig. 3.

To calculate the 3^1B^4 levels, the energies of the basis states of the 3^1B^n polyads, $n = 0$–3, were reduced to a set of vibrational parameters where the anharmonicity in ν_3' is folded into effective bending parameters. These parameters, which are listed below Table 6, were then used to calculate the rotational structure. A comparison of the observed and calculated level structures of the $2^13^1B^2$ and 3^1B^4 polyads is given in Table 6. Included in the data set are two levels, with $K' = 1$ and 3, which are not seen in the jet spectra, but which cause perturbations in the 3^4 level at higher J values; they are described in Ref. [48]. It can be seen that the match between the observed and calculated level positions is very good,

Table 6
Calculated and observed K-structures of the $2^13^1B^2$ and 3^1B^4 polyads of the $\tilde{A}^1A_u$ state of acetylene. For the $K' = 1$ levels the second entry is the value of B–C. Values in cm^{-1}.

Calculated[a]				Observed[b]			
$K' = 0$	$K' = 1$	$K' = 2$	$K' = 3$	$K' = 0$	$K' = 1$	$K' = 2$	$K' = 3$
46347 a_g	46434 0.003	46550		–	46434.4 0.003	46559.2	
46343 b_g	46284 0.006	46314	46413	–	46294.5[d] ∼0	–	46419.7[d]
46211 a_g	46238 0.060	**46255**[c]		46209.7	46240.2[e] 0.061	–	
46150 b_g	**46177** 0.024	46247		46153.3[f]	**46176.3** 0.033	46239.6[e]	
46133 a_g	46152 0.234[g]	46172		**46129.5**	46152.2 −0.239	46174.0	
46116 b_g	**46103** −0.030	**46122**		–	**46097.0** −0.017	**46121.3**	
46074 a_g	46081 −0.002[g]	46100		46075.4	46086.8 0.067	–	
46059 a_g	**46067** 0.056	**46079**		**46058.7**	**46068.5** 0.060	–	

[a] Parameters for calculation of 3^1B^4 levels: $K_{4466} = -57.86$, $\omega_4' = 752.00$, $\omega_6' = 742.47$, $x_{44}' = -0.405$, $x_{46}' = 15.425$, $x_{66}' = -3.695$, $y_{444}' = 0.173$, $y_{446}' = -0.55$, $y_{466}' = 1.245$, $y_{666}' = -0.798$, $A = 14.0$ cm^{-1}, $\zeta_{46}^a = 0.7028$.
[b] Values for $K > 0$ extrapolated to "$J = 0$".
[c] Values in bold face type belong to the $2^13^1B^2$ polyad.
[d] Values from deperturbation of avoided crossings in 3^4 (see Ref. [48]).
[e] Very strongly Coriolis-coupled.
[f] Vibrational b_g level, obtaining its intensity from the $K' = 1$ level at 46152.2 cm^{-1} by b-axis coupling.
[g] See text.

Table 7
Rotational constants for the $2^13^1B^2$ and 3^1B^4 polyads from band-by-band least squares fits. Values in cm^{-1}.

K'	T_0	½(B + C)	q[c]	D	r.m.s.
$2^13^1B^2$					
0*f*	46058.69 ± 0.04	1.0540 ± 0.0025			0.018
1	46068.47 ± 0.02	1.0258 ± 0.0018	0.0302 ± 0.0020		0.011
1	46097.00 ± 0.14	1.0025 ± 0.0129	−0.0084 ± 0.0046	−0.00026 ± 0.00024	0.064
2	46121.31 ± 0.03	1.0813 ± 0.0018			0.011
0*f*	46129.50 ± 0.17	1.1136 ± 0.0125		0.000057 ± 0.000056	0.073
1	46176.28 ± 0.06	1.0811 ± 0.0021	0.0163 ± 0.0027		0.047
3^1B^4					
0*f*	46075.38 ± 0.05	1.0646 ± 0.0031			0.023
1	46086.84 ± 0.04	1.0437 ± 0.0010	0.0333 ± 0.0014		0.034
1*e*	46151.94[a] ± 0.32	0.8987 ± 0.0507		−0.0022 ± 0.0015	0.092
1*f*	46152.48 ± 0.11	1.0183 ± 0.0178		−0.00046 ± 0.00054	0.033
0*e*	46153.30[a] ± 0.29	1.1847 ± 0.0460		0.0022 ± 0.0014	0.083
2	46174.04 ± 0.03	1.0639 ± 0.0037	0.00012 ± 0.00004	0.00012 ± 0.00009	0.009
0*f*	46209.70 ± 0.05	1.1039 ± 0.0015			0.026
2	46239.59[b] ± 0.21	0.8718 ± 0.0364	0.00035 ± 0.00025	−0.0016 ± 0.0014	0.025
1	46240.16[b] ± 0.34	1.1368 ± 0.0241	0.0306 ± 0.0116	0.0004 ± 0.0004	0.164
1	46434.40 ± 0.03	1.0099 ± 0.0013	0.0015 ± 0.0017		0.019
2	46559.23 ± 0.04	1.0342 ± 0.0094	−0.0004 ± 0.0005		0.019

[a] Strong *b*-axis Coriolis coupling between these levels leads to uncertainties in the parameters; the $K' = 1e$ and $1f$ levels have been fitted separately.
[b] Strongly interacting levels; the parameters are not well determined.
[c] The *K*-doubling has been taken as $\pm\frac{1}{2}q[J(J+1)]^K$ for the *e*/*f* levels; *q* corresponds to ½(*B*–*C*) for the $K' = 1$ levels.

with 12 of the 18 observed levels predicted to within 3 cm^{-1}, and the other six predicted to within 10 cm^{-1}.

Confirmation of the $K' = 1$ assignments comes from the asymmetry splittings, where the observed and calculated values of the asymmetry parameter *B*–*C*, listed in Table 6, are seen to agree to within about 0.01 cm^{-1}. At first sight it may seem that there are two exceptions to this statement, but there are simple explanations for them. One of the exceptions is the 46152.2 cm^{-1} level, where the calculations predict the large magnitude of *B*–*C* correctly, but with the wrong sign. The reason is that the nearby $K' = 0$ level, which causes the large splitting (by *b*-axis Coriolis coupling), is calculated to lie just below it, rather than just above it. Since the *b*-axis coupling is almost a first-order effect in this instance, the correct magnitude but incorrect sign follow at once.

The other exception is the lowest $K' = 1$ level of the 3^1B^4 polyad, at 46086.8 cm^{-1}, where the calculation predicts $B–C = -0.002$ cm^{-1} while the observed splitting gives $B–C = 0.067$ cm^{-1}. It turns out that the reason for the discrepancy is that the calculation places this $K' = 1$ level 5.5 cm^{-1} too low. We find that the apparent asymmetry splitting in the lowest $K' = 1$ level of a B^4 polyad is a very sensitive function of the energy separation between it and the lowest $K' = 0$ level. When the input parameters for the calculation are adjusted so that the "$J = 0$" energies of the two levels are reproduced exactly, the calculated value of *B*–*C* changes to 0.069 cm^{-1}, in excellent agreement with the observed value.

No attempt has been made to obtain a full least squares fit to the nine interacting vibrational levels, comparable to that in Table 2: the data are by no means as complete, while preliminary fits to the individual polyads show that many correction terms would have to be added to cope with the v'_3/v'_6 anharmonicity effects. Instead, band-by-band fits have been carried out. The resulting parameters are given in Table 7, and the assigned reduced rotational levels are shown plotted against $J(J + 1)$ in Fig. 11.

Fig. 12 illustrates two elegant examples of Coriolis coupling from the 3^1B^4 polyad. One is the pair of $K' = 0$ and 1 levels near 46153 cm^{-1}, discussed above. The $K' = 0$ level has b_g vibrational symmetry, which is an unusual observation. In other *gerade* bending polyads the $K' = 0$ levels of b_g vibrational symmetry are not seen because transitions to them are forbidden by the symmetry selection rules. However, in this instance the strong *b*-axis coupling transfers intensity to the $K' = 0$ sub-band, and generates an apparent asymmetry splitting in the $K' = 1$ level that is more than twice as large as that in the zero-point level. The b_g vibrational symmetry of the $K' = 0$ stack (*e* rotational symmetry) follows at once from the P- and R-branch structure of the $K' = 0–0$ sub-band. The other example illustrated is the pair of $K' = 1$ and 2 levels near 46239.5 cm^{-1}. For zero rotation these lie within 0.6 cm^{-1} of each other, and repel each other exceptionally strongly. The asymmetry splitting of this $K' = 1$ level is not affected by the interaction, and is calculated correctly.

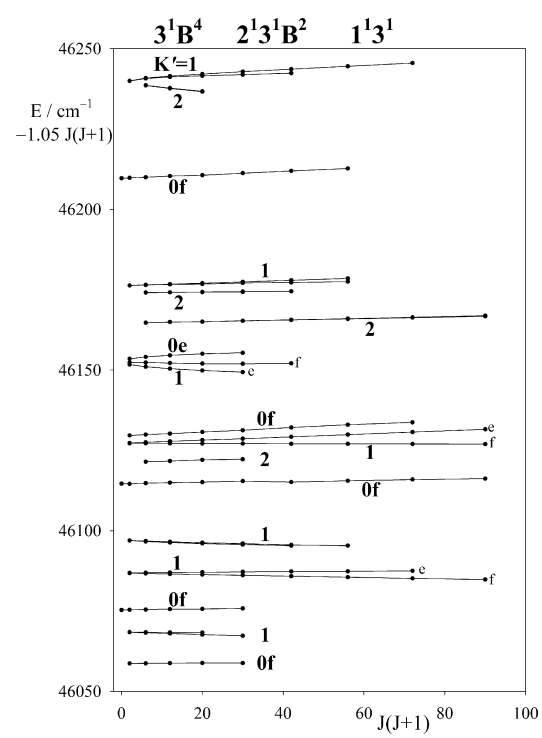

Fig. 11. Observed rotational levels of the 1^13^1, $2^13^1B^2$ and 3^1B^4 vibrational states, less 1.05 $J(J + 1)$, plotted against $J(J + 1)$. The lines in the figure are drawn only to guide the eye because a full least squares fit has not been carried out. The four highest assigned vibrational states are not shown. These are the $K' = 1$ state at 46294.49 cm^{-1} and the $K' = 3$ state at 46419.67 cm^{-1} (both of which perturb 3^4), the topmost $K' = 1$ state (46434.37 cm^{-1}) and the topmost $K' = 2$ state (46559.22 cm^{-1}).

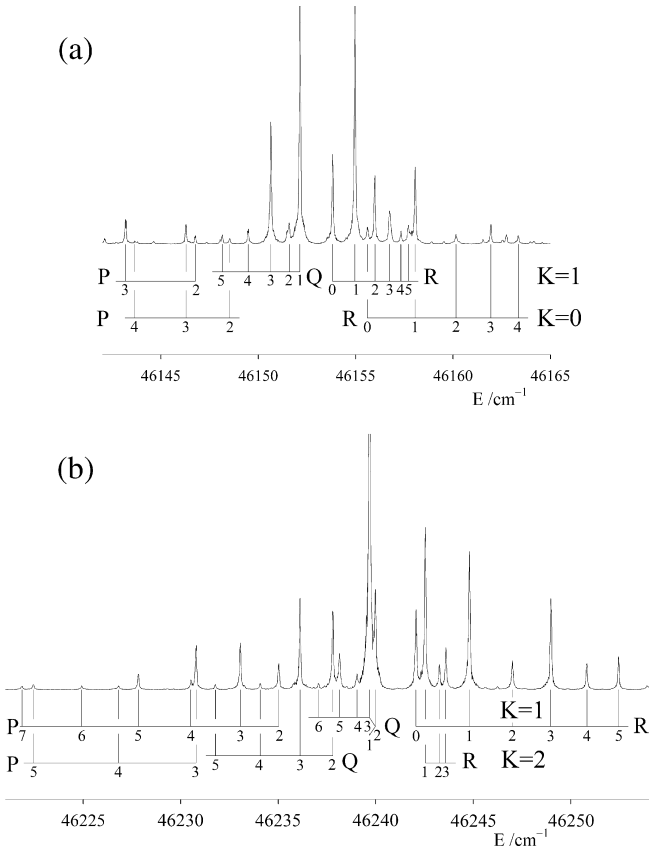

Fig. 12. Coriolis interactions in the 3^1B^4 polyad of acetylene. (a) Interacting $K' = 0$ (b_g) and $K' = 1$ levels near 46150 cm^{-1}; transitions to the $K' = 0$ (b_g) upper state are forbidden by the vibrational selection rules, but are induced by *b*-axis Coriolis interaction with the $K' = 1$ level. (b) Interacting $K' = 1$ and 2 levels near 46240 cm^{-1}; the two *K* stacks are almost degenerate for zero rotation. The spectra in (a) and (b) are at the same horizontal scale.

Not counting the 3^4, 2^3 and 1^13^1 levels (which have been reported elsewhere [41,42,48]), and the lowest $K' = 1$ component of 2^2B^2 at 46419 cm^{-1}, the structure listed in Table 6 accounts for every observed level in this region except for a $K' = 1$ level at 46192.20 cm^{-1} (mentioned above) and a $K' = 0$ (a_g) level at 46113.78 cm^{-1}. These two appear to be "extra" levels, since no other S_1-*trans* levels are expected in the region.

6.6. The 5^1B^1 polyad

Just to the high energy side of the intense 45811 cm^{-1} band (3^24^2, $K' = 1$), and partially overlapping the hot bands of the 2^2B^2 polyad, is a comparatively weak $K' = 1$ sub-band which can be identified as belonging to the 5^1B^1 polyad. It is illustrated in Fig. 9.

The 5^1B^1 polyad should have two components, 4^15^1 and 5^16^1, with vibrational symmetries b_g and a_g, respectively. The "$J = 0$" energy of the observed upper state is 45839.52 cm^{-1} (T_{00} + 3641.95 cm^{-1}), and the sense of its asymmetry splitting is that the *e*-symmetry component lies above the *f*-component, with an apparent value of $B–C = 0.045$ cm^{-1}. This value of $B–C$ is about half what would be expected for a level that is free from Coriolis effects, and shows that the upper state is part of a bending polyad. Since the position of the band rules out a combination involving ν'_1, ν'_2 or ν'_3, the only other combinations that could appear in one-photon laser excitation spectra according to the *g*–*u* selection rules are those involving the antisymmetric CH stretching vibration ν'_5 (b_u) with the *ungerade* bending vibrations. The sum of the ν'_5 frequency (2857.47 cm^{-1} [40]) and the mean of the two bending frequencies, ν'_4 and ν'_6 [39], is 3624.05 cm^{-1}, so that the observed band has to be the upper $K' = 1$ sub-band of the 5^1B^1 polyad. The sense of the asymmetry splitting, which is consistent with a vibrational level of a_g symmetry, indicates that the upper state has the zero order vibrational assignment 5^16^1. The energy order of the vibrational components of the 5^1B^1 polyad, with 5^16^1 above 4^15^1, is the same as the energy order of the fundamentals and the 2^1B^1 polyad, where the 2^16^1 level lies above the 2^14^1 level.

We are not able to assign the lower $K' = 1$ sub-band from our spectra. Assuming that the Coriolis coupling parameters are similar to those in other B^1 polyads, this band should lie near 45801 cm^{-1}. There are a few weak lines in this region, but it is not possible to pick out definite branches in between the very intense P and Q lines of the 45811 cm^{-1} band. With only one sub-band observed little more can be said about the 5^1B^1 polyad, except that it lies slightly lower than expected; the sum of the x'_{45} and x'_{56} parameters is roughly 25 cm^{-1}. The upper state term values of the observed levels are included in the Appendix.

6.7. ^{13}C Isotope shifts of the $K' = 1$ sub-bands

For some of the strong $K' = 1$ sub-bands, particularly those involving excitation of the C–C stretching vibration, ν'_2, it is possible to assign the corresponding bands of $H^{13}C^{12}CH$ in natural abundance. A clear example is the 2^2_0 band, illustrated in our earlier paper [41]. To our knowledge this was the first observation of a level of the $\tilde{A}$ state of $H^{13}C^{12}CH$, although its electronic ground state has been extensively studied. Table 8 lists the bands of $H^{13}C^{12}CH$ that have been identified in this work, and the corresponding isotope shifts. The largest isotope shifts are found for bands where quanta of ν'_2 are excited. It is fairly easy to pick out the $H^{13}C^{12}CH$ bands in these cases because they have no intensity alternation and the isotope shifts bring them well clear of the strong low-*J* P lines of the main bands, which are usually saturated under conditions where the $H^{13}C^{12}CH$ lines are observable. Since the saturated lines are often very wide, it can be difficult to pick out branches in the gaps between them. For bands with smaller isotope shifts it is not always straightforward to distinguish the isotopic lines from the axis-switching sub-bands [49] which lie in the same region. These latter are $\Delta K = 0$ sub-bands that arise because of a small rotation of the inertial axis system on electronic excitation. In particular, the strong Franck–Condon-allowed $K = 1–0$ sub-bands of the principal progressions always have a $K = 0–0$ axis-switching sub-band just below them, separated from them by the rotational constant $A - ½(B + C)$.

Three of the bands for which the isotope lines were easy to identify go to the levels 4^2, 3^14^2 and 3^24^2. These are comparatively intense isolated bands and, since they are the highest $K' = 1$

Table 8
^{13}C Isotope shifts for the $K' = 1$ sub-bands of the $\tilde{A}$–$\tilde{X}$ system of acetylene identified in this work. Values in cm^{-1}.

Assignment	T_0	$\Delta\nu$ ($H^{12}C^{12}CH$–$H^{13}C^{12}CH$)	
4^2	43801.77	−5.10	
2^13^1	44622.26	22.20	
3^14^2	44810.71	0.43	
2^2	44920.46	39.91	(Ref. [41])
2^13^2	45644.49	32.09	
3^24^2	45805.16	5.4_3	(^{12}C perturbed)
2^23^1	45962.58	45.58	
1^13^1	46125.54	1.61	
3^4	46274.20	13.9_9	(perturbed)
1^12^1	46453.92	21.07	
2^13^3	46654.53	32.3_9	(^{12}C perturbed)

The T_0 values refer to the bands of $H^{13}C^{12}CH$.
Derived shifts per quantum: ν'_1: 3.8 cm^{-1}; ν'_2: 23.4 cm^{-1}; ν'_3: 5.3 cm^{-1}; ν'_4: 0.9 cm^{-1}.
Zero point level shift ($K' = 1$): −6.8 cm^{-1}.
A very weak band at 46049.07 cm^{-1} appears to be the ^{13}C analog of the $2^13^1B^2$ band at 46068.47 cm^{-1}, though the assignment is not certain.

members of B^2 polyads, where the K-structure is distorted by the a-axis Coriolis interaction, they have no accompanying $K = 0$–0 axis-switching sub-bands. We have also identified the 3^4_0 band of $H^{13}C^{12}CH$. The reason for interest in this band was to locate a component of the 3^1B^4 polyad which is predicted to lie nearby. Because of the great intensity of the 3^4_0 band and its axis-switching structure, special experiments with a seeded beam were carried out in order to cool the acetylene as much as possible. It turns out that the 3^4_0 band of $H^{13}C^{12}CH$ contains triplet perturbations at low J values, of the type identified by Drabbels et al. [7] in the 3^3 and 3^4 levels of $H^{12}C^{12}CH$. As a result it is only possible to give an approximate value for the isotope shift.

Comparison of the shifts in Table 8 shows that, with the exception of that for 2^13^2, the observed shifts are additive to within 1–2 cm^{-1}. Discounting the 2^13^2 level, where the line assignments are not in doubt, but the isotope shift is anomalous for reasons that we do not understand, the values in Table 8 allow the shifts per quantum to be derived for v'_1 through v'_4; these are listed below the table, along with the electronic isotope shift. The derived shifts agree quite closely with the values we calculate from the harmonic force field of Tobiason et al. [40] For example, the shift per quantum of v'_2 (23.38 cm^{-1}) compares well with the harmonic force field value (23.1 cm^{-1}). For v'_3 the harmonic force field value (7.9 cm^{-1}) is possibly slightly too large, since the majority of the numbers in Table 8 indicate a shift per quantum of close to 5.3 cm^{-1}.

It can be argued that the shift per quantum for v'_4, which has been derived from levels of B^2 polyads where Darling–Dennison resonance is known to be strong, should be corrected for the effects of this resonance. In fact any such correction must be very small, since the v'_4 and v'_6 vibrations have almost the same frequency, and their harmonic force field isotope shifts are calculated to be the same to within 0.1 cm^{-1}. Different degrees of mixing of the v'_4 and v'_6 basis states caused by the Darling–Dennison resonance will therefore have almost no effect on their isotope shifts.

7. Discussion

This work was motivated by *ab initio* calculations [1,5] that the S_1 state of acetylene has a comparatively low barrier to *trans–cis* isomerization of about 4700 cm^{-1}. Only the *trans* well of the S_1 state ($\tilde{A}^1A_u$) is observable spectroscopically, since the *cis* well transforms as $^1A_2$, to which absorption transitions from the ground electronic state are forbidden. Nevertheless, the possibility exists that levels of the *cis* well near the top of the barrier can tunnel through it and give rise to observable bands, picking up intensity by interaction with nearby *trans*-well levels. Obviously a search for levels of this type requires a very detailed and complete understanding of the level structure of the $\tilde{A}$ state in order to identify any "extra" level that does not belong to the *trans* isomer. With this aim in mind we report rotational analyses of a number of newly-discovered vibrational bands at the long wavelength end of the $\tilde{A}$–$\tilde{X}$ system of acetylene. Specifically we have focused on the combination levels involving the a_g vibrations of the $\tilde{A}$ state with the low-lying bending vibrations, v'_4 and v'_6. Together with the results from previous work [35–43], analyses are now available for some parts of more than 75 vibrational levels of the $\tilde{A}$ state, including every predicted level up to a vibrational energy of 3500 cm^{-1}. Four suspected *cis*-well levels have been found, but further studies are required to confirm their identities and give their vibrational assignments.

There are various reasons why such a complete cataloguing of the vibrational structure has been possible. On the experimental side the main reason has been the very large dynamic range of the recorded spectra, which results from the way the laser-induced fluorescence has been gated so as to minimize the scattered laser light. Without this, the very weak bands at the long wavelength end of the band system would never have been detected. We have also made certain that full rotational analyses were carried out for those bands where pattern recognition methods break down because of the complexity of the rotational structure. In these cases the rotational assignments were made by stimulated emission pumping and population labeling experiments. On the theoretical side, we have gone to some length to understand the details of the Coriolis and Darling–Dennison resonances, which have allowed us to obtain good quality constants from the lower energy bending polyads that could be used to predict, reasonably accurately, the structures of some of the higher bending polyads. For the purpose of understanding these details it has been essential to put equal weight on data from the one-photon UV spectra and the IR–UV double resonance spectra, since g–u symmetry considerations cause the members of a B^n progression to alternate between the two types of spectra. However probably the most important reason for the completeness of the results is the emphasis we have placed on obtaining spectra of the $K' = 0$ and 2 rotational levels, both in the one-photon and the double resonance experiments. The C-type rotational selection rules ($K' - \ell'' = \pm 1$) strongly favor the collection of $K' = 1$ data, whether in cold jet one-photon spectra from the $v'' = 0$ level or via the intense v''_3 fundamental in double resonance, but without $K' = 0$ and 2 data it would have been quite impossible to understand the Coriolis effects, and therefore to make any sensible predictions of the structure at higher energy.

The most interesting result from the present work has been the surprising anharmonicity in the combinations of v'_3 (*trans* bend, a_g) and v'_6 (in-plane *cis* bend, b_u). This is shown very clearly by the structures of the 3^nB^2 polyads. Fig. 13 illustrates the three $K' = 1$ sub-bands of the 3^nB^2, $n = 0$–3 polyads, showing how the compact structure of the B^2 polyad opens up with excitation of v'_3. (The lowest frequency component of 3^3B^2 has not been securely identified yet, but probably lies near 46550 cm^{-1}.) The high frequency members of the polyads, nominally 3^n4^2, form a normal progression with regularly decreasing spacing, but the low frequency members (3^n6^2) drop rapidly below the rest of the polyad: for example, the separation of the two lower $K' = 1$ sub-bands increases from 9 cm^{-1} in B^2 to 73 cm^{-1} in 3^2B^2. It is not easy to obtain the vibrational energies directly from the positions of the $K' = 1$ levels because of the Darling–Dennison and Coriolis resonances, but deperturbed values are given by the least squares fits of Tables 3 and 4 and Ref. [43]. The results show that, while the 4^2 level lies 2.09 cm^{-1} above the 6^2 level in zero-order, the 3^24^2 level lies 102.91 cm^{-1} above the 3^26^2 level in zero-order.

The shape of the molecule at the *trans–cis* isomerization barrier is calculated to be half-linear [1,5], which would correspond to simultaneous excitation of the v'_3 and v'_6 vibrations. Clearly the anharmonicity represents the molecule approaching the barrier, presumably with a change in the nature of the vibrational coordinates, which contributes to the variation of K_{4466} with v'_3. The need for the many small correction terms in the least squares fits to the combination polyads, particularly $2^13^1B^1$ and 3^1B^3, must arise from the same cause.

The resonance parameters $2A\zeta^a_{46}$ and K_{4466} increase unexpectedly quickly with excitation of v'_3. For example, the fitted value of $2A\zeta^a_{46}$ rises from 18.45 cm^{-1} in the B^2 polyad to 23.56 cm^{-1} in the 3^2B^2 polyad. However this increase is not related to the v'_3/v'_6 anharmonicity (since the Coriolis constants are independent of the force field), but arises instead from the increase in the average HCC bond angle with excitation of v'_3. With $r_{CC} = 1.375$ Å and $r_{CH} = 1.097$ Å [50], the effective HCC bond angles for the members of the v'_3 progression can be calculated from the A rotational constants reported by Watson et al. [37] The ζ_{46} constants corresponding to these angles can then be obtained by standard methods [51,52]. For $v'_3 = 0$ and 2 the calculated values of ζ^a_{46} are 0.680 and 0.736, giving $2A\zeta^a_{46} = 17.76$ and 22.32 cm^{-1}, respectively.

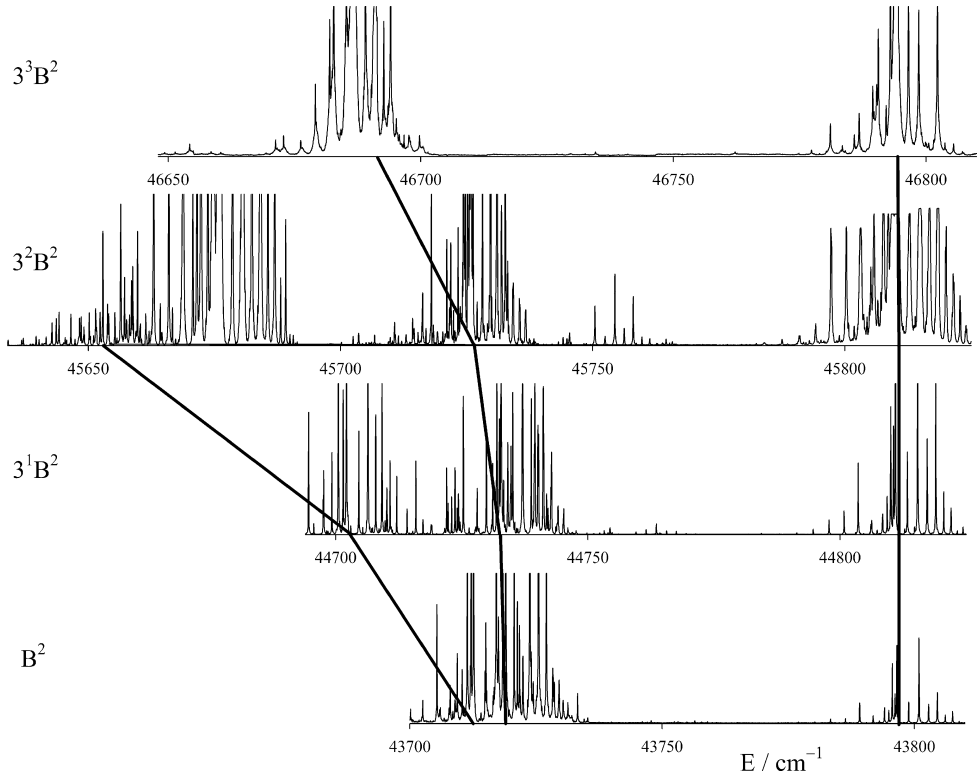

Fig. 13. Jet-cooled excitation spectra showing the three $K' = 1$ sub-bands of each of the 3^nB^2, $n = 0$–3 polyads. (The lowest energy sub-band of 3^3B^2 has not been definitely identified yet.) The spectra are all to the same horizontal scale, and arranged so that the highest frequency sub-bands (nominally 3^n4^2) are aligned vertically. Thick lines join the positions of the sub-band origins. The assignments of the overlapping bands are not marked.

(The factor of Ω in Eq. (1) has been ignored since, for $v_3 = 2$, the effective value of Ω differs from 1 by only 0.07%.) Although these calculated values are slightly smaller than the observed, the trend is reproduced correctly: the large increase in $2A\zeta^a_{46}$ with v'_3 occurs because both A and ζ^a_{46} increase as the molecule becomes more nearly linear.

The Darling–Dennison parameter, K_{4466}, depends on the force field as well as on the A and B rotational constants and the Coriolis ζ parameters. To second-order [53] it is given by

$$K_{4466} = \frac{1}{4}\phi_{4466} - 4[A(\zeta^a_{46})^2 + B(\zeta^b_{46})^2]\Omega^2 + \frac{1}{8}\sum_k \phi_{k44}\phi_{k66}\omega_k[(4\omega_4^2 - \omega_k^2)^{-1} + (4\omega_6^2 - \omega_k^2)^{-1}]. \quad (9)$$

The methods of the previous paragraph allow the Coriolis contribution to be calculated. The Coriolis effects account for only about two thirds of the change in the value of K_{4466} with v'_3, which implies that the second-order expression is beginning to break down. Specifically, the fitted values of K_{4466} for the B^2 and 3^2B^2 polyads are −51.68 and −66.50 cm^{-1}, respectively, while the calculated values of $-4[A(\zeta^a_{46})^2 + B(\zeta^b_{46})^2]\Omega^2$ for $v'_3 = 0$ and 2 are −28.48 and −38.73 cm^{-1}. It is remarkable that the Coriolis effects make up more than half the value of K_{4466}, and also that this fraction increases with v'_3.

Several perturbations attributed to triplet electronic states have been identified in the course of this work. A summary of the most prominent perturbations is given in Table 9. Of the states that manifest splitting of the observed lines, anomalously long fluorescence lifetimes, or significant zero-field quantum beats, most have been subsequently studied by a combination of time-gated fluorescence and SEELEM (surface electron ejection by laser-excited metastables) techniques, demonstrating a variety of dynamics associated with vibrational state-specific intersystem crossing [54].

Table 9
Summary of Ã-state vibrational levels believed to be perturbed by triplet states in the absence of a magnetic field. Evidence (apart from observable splitting in the LIF spectrum) for the nature of the perturbation is provided by the experiments listed in the rightmost column. No claim of completeness is made, as the existing experiments are biased towards the strongest transitions and those perturbations observable at low J.

T_0	Assignment	Experiments
45300	3^3, $K' = 1$	High-resolution LIF[a], Zeeman quantum beats[b], SEELEM[c]
45347	3^3, $K' = 2$	SEELEM[d]
45423	3^3, $K' = 3$, $J' = 3$–6, 8	
45676	2^13^2, $K' = 1$	SEELEM[d]
46008	2^23^1, $K' = 1$	SEELEM[d]
46288[e]	3^4, $K' = 1$	High-resolution LIF[a], Zeeman quantum beats[b]
44811[f]	3^1B^2, $K' = 1$, III, $J' = 2e$	Zero-field quantum beats
45811[g]	3^2B^2, $K' = 1$, III	SEELEM[d]
46192	"Extra" $K' = 1$	SEELEM[h]
45539[i]	3^1B^3, $K' = 0f$, II	
45938	3^3B^1, $K' = 0f$	SEELEM[d]
45947	3^3B^1, $K' = 1$, I	Zeeman quantum beats[j]
46040	3^3B^1, $K' = 0e$	SEELEM[d]

SEELEM, surface electron ejection by laser-excited metastables.
Roman numerals represent energy rank of a given K sublevel within a polyad.
[a] Ref. [7].
[b] Ref. [55].
[c] Ref. [13].
[d] Ref. [54].
[e] Triplet perturbations also noted in $H^{13}C^{12}CH$: see Section 6.1.
[f] See Section 6.1.
[g] See Section 6.2.
[h] Ref. [14]. This state was preliminarily assigned as $2^13^1B^2$, $K' = 1$, III. See analysis in Section 6.5 for reassignment.
[i] See Section 5.2.
[j] Ref. [11].

A number of exciting avenues for future work are suggested by the present results. One of the most interesting will be the vibrational assignment of the "extra" vibrational levels that have no place in the manifold of the S_1-*trans* state. Already we have found that the $H^{13}C^{12}CH$–$H^{12}C^{12}CH$ isotope shift of the "extra" level at 46192 cm^{-1} is completely at odds with its apparent position in the *trans* well, suggesting that it lies at quite low energy in a state whose potential minimum lies above that of the *trans* well. A combination of isotope data with vibrational symmetry arguments based on the rotational selection rules should allow assignments to be made, and give an estimate of the relative energies of the *cis* and *trans* wells. After that comes the problem of exactly what is the energy of the *trans–cis* isomerization barrier. The 46192 cm^{-1} "extra" level, which is the highest-energy "extra" level that we have found, appears to have an even–odd staggering in its *K*-structure, of the type expected for tunneling through the barrier. The size of the staggering will be related to the classical frequency of this tunneling, carrying information about where the level lies relative to the top of the barrier. The spectra become increasingly confused in this energy region and the effects of predissociation start to become troublesome but, with careful systematic analyses, progress should be possible.

Acknowledgments

We thank Dr. J.K.G. Watson (N.R.C., Ottawa) for providing the unpublished line measurements for the perturbed 2^13^1 $K' = 3$ sub-bands, and Annelise Beck for assistance with the collection of the data at MIT. We also thank Z. Duan and D. Oertel for allowing us access to their unpublished results on the fluorescence observed from the 3^2B^2 polyad. The work at MIT was supported by DOE Grant no. DE-FG0287ER13671. AJM thanks the Natural Sciences and Engineering Research Council of Canada, and ST thanks the National Science Council of Taiwan, for partial support of this work.

Appendix

Upper state term values for the assigned stretch-bend combination polyads of the $\tilde{A}^1A_u$ state of acetylene. Values in cm^{-1}. Roman numerals distinguish *K*-stacks of the same *K*-value in a polyad in order of increasing energy. Term values not used in the fits are marked with an asterisk.

A. The 2^1B^1 polyad.

J	*K* = 0*e* (2^14^1)	*K* = 1*e* (I)	*K* = 1*e* (II)	*K* = 2*e* (I)	*K* = 2*e* (II)	*K* = 3*e* (I)
e-symmetry						
1	44338.47_5	44335.53	44373.80			
2	343.18	339.16	378.16	44357.87	44431.25	
3	349.97	344.84	384.67	364.40	437.73	44405.29
4	358.83	352.57	393.39_5	373.13	446.30	
5	369.68	362.44	404.29	383.97	456.99	
6		374.31	417.33	396.97	469.81	
7		388.56	412.13		484.89	
8					502.02	
9					521.38	
J	*K* = 0*f* (2^16^1)	*K* = 1*f* (I)	*K* = 1*f* (II)	*K* = 2*f* (I)	*K* = 2*f* (II)	*K* = 3*f* (I)
f-symmetry						
0	44345.72					
1	347.97	44335.84	44373.77			
2	352.38_5	339.68_5	378.08	44357.91	44431.27_5	
3	358.91	345.62	384.49	364.50	437.71	44405.29
4	367.54_5	353.53_5	393.06	373.37	446.29_5	413.87
5	378.13_7	363.49_5	403.79	384.47_5	457.02	424.60
6	390.86	375.54		397.86	469.89_5	437.47
7	405.34	389.74		413.49	484.90	452.49
8		406.00		431.36	502.08	
9				451.31		

B. The $2^13^1B^1$ and 3^1B^3 polyads.

J	*K* = 1*e* (I)	*K* = 0*e* ($2^13^14^1$)	*K* = 2*e* (I)	*K* = 1*e* (II)	*K* = 3*e* (I)	*K* = 2*e* (II)	*K* = 3*e* (II)
$2^13^1B^1$, e-symmetry							
1	45360.34	45371.66_5		45407.12_5			
2	364.25_3	376.08	45382.69	411.35		45465.15_5	
3	370.16_7	382.67	389.25_5	417.66_5	45431.88	471.57	45554.79
4	378.12_5	391.28	398.03	426.12	440.41	480.11	563.34
5	388.10_5	401.98	409.06	436.63	451.06	490.70_5	574.07
6	400.22				463.82*	504.60	586.91
7	414.39					519.42	

(*cotinued on next page*)

Appendix (*continued*)

J	$K = 1f$ (I)	$K = 0f$ ($2^1 3^1 6^1$)	$K = 2f$ (I)	$K = 1f$ (II)	$K = 3f$ (I)	$K = 2f$ (II)	$K = 3f$ (II)
$2^1 3^1 B^1$, f-symmetry							
0		45362.98					
1	45360.16	365.29		45407.05			
2	363.93	369.83	45382.68	411.35		45465.18_5	
3	369.68_5	376.54	389.22	417.68	45431.89	471.62	45554.79
4	377.46_7	385.31	397.94	426.08	440.42	480.18_5	563.38
5	387.30_5	396.14	408.87	436.60*	451.06	490.83_5	574.02
6	399.28	408.93_5	421.94	449.23*	463.80*	505.29	586.90
7		423.76			478.44*		601.92
8		440.57			495.39*		
J	$K = 1e$ (I)	$K = 0e$ (I)	$K = 2e$ (I)	$K = 1e$ (II)	$K = 2e$ (II)	$K = 3e$ (II)	$K = 4e$ (I)
$3^1 B^3$, e-symmetry							
1	45399.11_3	45446.36		45463.55_5			
2	403.35_5	450.81	45427.36	467.56_5	45477.70		
3	409.67_7	457.30	433.67	473.68_7	483.78	45507.60	
4	418.16	466.08	442.05	481.87_5	491.97	514.77	45519.78
5	428.77	477.02_5		492.11	502.37	524.59	531.05
6		490.04		503.24		536.70	543.94
7		507.28		517.60		551.10	558.76
J	$K = 1f$ (I)	$K = 0f$ (I)	$K = 2f$ (I)	$K = 1f$ (II)	$K = 2f$ (II)	$K = 3f$ (II)	$K = 4f$ (I)
$3^1 B^3$, f-symmetry							
0		45397.78		45463.57			
1	45398.89	400.09		467.80_5			
2	402.78_5	404.60	45427.38	474.01	45477.67		
3	408.78	411.29	433.66	482.38	483.81_5	45507.61	
4	416.89	420.05	442.07	492.78	492.10	514.79	45519.80
5	427.08_5	430.96		503.55	502.61	524.61	
6	439.39	443.97			515.35	536.75	543.91
7		459.09					
J	$K = 1e$ (III)	$K = 2e$ (III)	$K = 0e$ (II)	$K = 3e$ (III)	$K = 1e$ (IV)	$K = 2e$ (IV)	
$3^1 B^3$, e-symmetry							
1	45502.19		45548.15		45616.81		
2	506.62	45535.19	552.62		621.19	45719.10	
3	513.47	541.76_5	559.31	45623.17	627.75	725.57	
4	522.92	550.58	568.25	631.81	636.54	734.25	
5	535.21	561.52	579.45	642.55	647.43_5	745.13	
6	549.86		592.93	655.56	660.61	758.19	
7	566.76			670.65		773.45	
8						790.91	
J	$K = 1f$ (III)	$K = 2f$ (III)	$K = 0f$ (II)	$K = 3f$ (III)	$K = 1f$ (IV)	$K = 2f$ (IV)	
$3^1 B^3$, f-symmetry							
1			45540.63		45616.79_5		
2	45506.59	45535.17	545.18		621.18_5	45719.06	
3	513.39	541.75_5	551.89	45623.13	627.80	725.55	
4	522.87	550.50	560.89	631.80	636.63_5	734.26	
5	535.11	561.43	572.07_5	642.55		745.14	
6	549.78	574.51	585.60_5	655.56		758.19	
7			601.46	670.67		773.52	
8			619.54	688.00		790.91	

Appendix (*continued*)
C. The 3^1B^2 polyad.

J	$K = 1e$ (I)	$K = 2e$ (I)	$K = 1e$ (II)	$K = 2e$ (II)	$K = 1e$ (III)
3^1B^2, *e-symmetry*					
1	44704.61				44813.35_5
2	708.77_5	44724.38	44735.14	44761.91	817.75_5
3	715.04_5	730.07	739.44	768.63	824.35_5
4	723.36	737.79	745.85_5	777.74	833.11_5
5	733.71_5	747.63		789.16	844.11_5
6	746.10	759.65		802.86	857.32_5
7	773.88		818.90	872.71	44813.35_5
8				890.27_5	

J	$K = 0f$ (I)	$K = 1f$ (I)	$K = 2f$ (I)	$K = 1f$ (II)	$K = 2f$ (II)	$K = 0f$ (II)	$K = 1f$ (III)
3^1B^2, *f-symmetry*							
0						44764.84*	
1	44694.98_5	44704.49		44735.18		767.18_5	44813.32
2	699.18	708.57	44724.38	739.54	44761.90	771.61	817.69
3	705.62_5	714.67	730.06	746.06	768.54	778.39	824.18
4	714.10_5	722.80	737.71	754.67	777.54	787.38_5	832.88
5	724.79	732.94	747.44	765.21	788.54	798.54	843.79
6	737.54	745.09	759.25		801.77		856.76
7	752.41				817.07		

D. The 2^1B^2 polyad.

J	$K = 1e$ (I)	$K = 2e$ (I)	$K = 1e$ (II)	$K = 2e$ (II)	$K = 1e$ (III)
2^1B^2, *e-symmetry*					
1	45080.59		45089.69_5		45164.44
2	084.81_5	45091.88	095.53_5	45121.80_5	168.79_5
3	091.05_5	096.64	102.17_5		175.35_5
4	099.15	103.60_3	110.95	137.08	184.07_5
5	108.83		121.86_5		194.99_5
6	120.11		134.85_5		208.08
7			149.89		223.41
8					240.86

J	$K = 0f$ (I)	$K = 1f$ (I)	$K = 2f$ (I)	$K = 1f$ (II)	$K = 2f$ (II)	$K = 0f$ (II)	$K = 1f$ (III)
2^1B^2, *f-symmetry*							
0	45067.23					45119.83	
1	069.36_5	45080.53		45089.66		122.06	45164.42
2	073.64_7	084.64	45091.87	095.35_3		126.53	168.74
3	080.04	090.81	096.41	101.76	45128.32	133.23	175.22
4	088.57_5	098.65	103.25	110.18_5		142.18	183.85
5	099.21	108.55	112.48	120.71		153.45_5	194.63
6	112.00_5		124.20				207.58
7	126.85_5						222.66

E. The 3^2B^2 polyad.

J	$K = 1e$ (I)	$K = 1e$ (II)	$K = 2e$ (II)	$K = 1e$ (III)
3^2B^2, *e-symmetry*				
1	45655.32_5	45728.15		45812.80_5
2	659.55	732.12	45752.78	817.22
3	665.89	738.10_5	759.54	823.81
4	674.38		768.60	832.53
5	684.96_5		779.84	843.60
6	697.70		793.38	856.87_5
7			809.24*	872.26
8				889.88

(*continued on next page*)

Appendix (*continued*)

J	$K = 0f$ (I)	$K = 1f$ (I)	$K = 1f$ (II)	$K = 2f$ (II)	$K = 0f$ (II)	$K = 1f$ (III)
3^2B^2, f-symmetry						
0	45644.18					
1	646.28_5	45655.26	45728.18		45768.87	45812.76
2	650.50	659.42	732.28	45752.79	773.28	817.18*
3	656.86	665.59	738.52	759.53	779.90	823.58
4	665.33	673.94	746.85	768.41	788.78	832.18
5	675.79*	684.36	757.21	779.42	799.84	842.98
6		696.80		792.63		855.21*
7				807.92*		

F. The $2^13^1B^2$ and 3^1B^4 polyads.

J	$K = 1e$ (I)	$K = 1e$ (II)	$K = 2e$ (II)	$K = 1e$ (III)
$2^13^1B^2$, e-symmetry				
1	46070.55	46099.05_5		46178.405
2	074.72_5	102.94	46127.79	182.79
3	080.96_5	108.91	134.29	189.315
4	089.29	117.02	143.055	198.02
5		127.18	153.745	208.935
6		139.44		222.03
7				237.31

J	$K = 0f$ (I)	$K = 1f$ (I)	$K = 1f$ (II)	$K = 2f$ (II)	$K = 0f$ (II)	$K = 1f$ (III)
$2^13^1B^2$, f-symmetry						
1	46060.78	46070.50	46099.08		46131.75	46178.41
2	065.01	074.52	103.09	46127.79	136.22	182.80
3	071.36	080.62	109.14	134.29	142.82	189.24
4	079.84	088.68	117.26	143.055	151.71	197.78
5	090.30	098.80	127.51	153.745	162.77	208.60
6			139.67		176.23	221.36
7			154.17		191.77	236.32
8					209.33	

J	$K = 1e$ (I)	$K = 1e$ (II)	$K = 0e$ (I)	$K = 2e$ (II)	$K = 2e$ (III)	$K = 1e$ (III)
3^1B^4, e-symmetry						
1	46088.965	46153.815	46155.597			46242.077
2	093.21	157.32	160.41	46180.42	46244.90	247.165
3	099.59	163.035	167.20	186.78	250.33	254.06
4	108.085	170.85	176.055	195.29	257.735	263.11
5	118.685	180.85	186.87	205.91		274.35
6	131.42			218.61		287.75
7	146.17					303.325
8	163.125					321.15

J	$K = 0f$ (I)	$K = 1f$ (I)	$K = 1f$ (II)	$K = 0f$ (II)	$K = 2f$ (II)	$K = 2f$ (III)	$K = 1f$ (III)
3^1B^4, f-symmetry							
0	46075.37			46209.68			
1	077.49	46088.88	46154.49	211.925			46242.05
2	081.758	092.99	158.65	216.32	46180.42	46244.86	247.04
3	088.19	099.14	164.77	222.967	186.78	250.24	253.82
4	096.65	107.35	173.01	231.63	195.24	257.61	262.57
5	107.31	117.63	183.45	242.765	205.79		273.44
6	088.965	129.95	196.20	256.07			286.48
7		144.33		271.53			
8		160.76					
9		179.33					

Appendix (*continued*)
G. The 2^2B^2 polyad.

J	$K = 1e$ (V)	$K = 2e$ (V)	$K = 1e$ (I)	$K = 1e$ (III)
3^1B^4, *e-symmetry*			*e-symmetry*	
1	46436.575		46421.07	46507.61
2	440.995	46565.41	425.09	511.96
3	447.61	571.61	431.06	518.46
4	456.41		438.94	527.11_5
5	467.44	590.12	448.68	537.95
6	480.64		460.29	550.97
7	496.01			566.07
8	513.36			

J	$K = 1f$ (V)	$K = 2f$ (V)	$K = 1f$ (I)	$K = 1f$ (III)	$K = 0f$ (IIa)	$K = 0f$ (IIb)
3^1B^4, *f-symmetry*			2^2B^2, *f-symmetry*			
0					46460.60	46467.84
1	46436.58		46421.03	46507.61	462.76_5	470.02
2	441.01	46565.45	425.02	511.88	467.18	474.31_5
3	447.59	571.66	430.93	518.29	473.87_5	480.81_7
4	456.39		438.79	526.83	482.86	489.49
5	467.36	590.26	448.62	537.51	494.05	500.38
6			460.39*	550.35	507.36*	
7			471.74	565.34	522.73 (Interaction with 1^12^1)	

H. Other bands.

	5^16^1		2^26^1		2^13^3	
J	$K = 1e$	$K = 1f$	$K = 0f$ (I)	$K = 2$ (II)	$K = 1e$	$K = 1f$
1	45841.71	45841.67	45705.00		46689.04_5	46689.02
2	846.10_5	845.97	709.31	45784.24	693.29	693.23
3	852.70	852.45	715.67	790.64_5	699.76	699.45
4	861.48	861.03	723.98	799.16	708.15	707.72
5	872.41	871.81		809.80	718.71	718.06
6	885.62			822.59	731.08_5	730.63
7				K-doubling not resolved	745.58	

	3^3B^2				46791 cm^{-1}	
J	$K = 1e$ (II)	$K = 1f$ (II)	$K = 1e$ (III)	$K = 1f$ (III)	$K = 1e$	$K = 1f$
1	46694.02*	46694.02	46796.53_5	46796.42	46792.90	46792.94
2	697.76_5	698.06*	800.90	800.79	797.32	797.31
3	703.78_5	704.33	807.56_5	807.10*	803.86	803.83
4	711.80_5	712.59*	816.39_5	815.67	812.64	
5	722.40	722.80*	827.54	826.37	823.54	
6	735.08		840.74		836.85	
7						

References

[1] J.F. Stanton, C.M. Huang, P.G. Szalay, Chem. Phys. Lett. 101 (1994) 356.
[2] Q. Cui, K. Morokuma, J.F. Stanton, Chem. Phys. Lett. 263 (1996) 46.
[3] Q. Cui, K. Morokuma, Chem. Phys. Lett. 272 (1997) 319.
[4] K. Malsch, R. Rebentisch, P. Swiderek, G. Hohlneicher, Theor. Chem. Acc. 100 (1998) 171.
[5] E. Ventura, M. Dallos, H. Lischka, J. Chem. Phys. 118 (2003) 1702.
[6] H. Köppel, B. Schubert, H. Lischka, Chem. Phys. 343 (2008) 319.
[7] M. Drabbels, J. Heinze, W.L. Meerts, J. Chem. Phys. 100 (1994) 165.
[8] S.J. Humphrey, C.G. Morgan, A.M. Wodtke, K.L. Cunningham, S. Drucker, R.W. Field, J. Chem. Phys. 107 (1997) 49.
[9] S. Altunata, R.W. Field, J. Chem. Phys. 113 (2000) 6640.
[10] M. Mizoguchi, N. Yamakita, S. Tsuchiya, A. Iwasaki, K. Hoshina, K. Yamanouchi, J. Phys. Chem. A 104 (2000) 10212.
[11] N. Yamakita, S. Tsuchiya, Chem. Phys. Lett. 348 (2001) 53.
[12] S. Altunata, K.L. Cunningham, M. Canagaratna, R.L. Thom, R.W. Field, J. Phys. Chem. A 106 (2002) 1122.
[13] A.P. Mishra, R.L. Thom, R.W. Field, J. Mol. Spectrosc. 228 (2004) 565.
[14] W.L. Virgo, K.L. Bittinger, A.H. Steeves, R.W. Field, J. Phys. Chem. A 111 (2007) 12534.
[15] M. Fujii, A. Haijima, M. Ito, Chem. Phys. Lett. 150 (1988) 380.
[16] A. Haijima, M. Fujii, M. Ito, J. Chem. Phys. 92 (1990) 959.
[17] D.H. Mordaunt, M.N.R. Ashfold, J. Chem. Phys. 101 (1994) 2630.
[18] D.H. Mordaunt, M.N.R. Ashfold, R.N. Dixon, P. Löffler, L. Schnieder, K.H. Welge, J. Chem. Phys. 108 (1998) 519.
[19] S.A.B. Solina, J.P. O'Brien, R.W. Field, W.F. Polik, J. Phys. Chem. 100 (1996) 7797.

[20] M.P. Jacobson, J.P. O'Brien, R.J. Silbey, R.W. Field, J. Chem. Phys. 109 (1998) 121.
[21] M.P. Jacobson, R.W. Field, J. Phys. Chem. A 104 (2000) 3073.
[22] K. Hoshina, A. Iwasaki, K. Yamanouchi, M.P. Jacobson, R.W. Field, J. Chem. Phys. 114 (2001) 7424.
[23] K. Tsuji, C. Terauchi, K. Shibuya, S. Tsuchiya, Chem. Phys. Lett. 306 (1999) 41.
[24] B.J. Orr, Int. Rev. Phys. Chem. 25 (2006) 655.
[25] D.M. Jonas, S.A.B. Solina, B. Rajaram, R.J. Silbey, R.W. Field, K. Yamanouchi, S. Tsuchiya, J. Chem. Phys. 99 (1993) 7350.
[26] D.J. Nesbitt, R.W. Field, J. Phys. Chem. 100 (1996) 12735.
[27] D.B. Moss, Z. Duan, M.P. Jacobson, J.P. O'Brien, R.W. Field, J. Mol. Spectrosc. 199 (2000) 265.
[28] M. Silva, R. Jongma, R.W. Field, A.M. Wodtke, Ann. Rev. Phys. Chem. 52 (2001) 811.
[29] J.K. Lundberg, Y. Chen, J.P. Pique, R.W. Field, J. Mol. Spectrosc. 156 (1992) 104.
[30] M. Takahashi, M. Fujii, M. Ito, J. Chem. Phys. 96 (1992) 6486.
[31] J.K. Lundberg, D.M. Jonas, B. Rajaram, Y. Chen, R.W. Field, J. Chem. Phys. 97 (1992) 7180.
[32] S.T. Pratt, P.M. Dehmer, J.L. Dehmer, J. Chem. Phys. 99 (1993) 6233.
[33] S.-J. Tang, Y.-C. Chou, J. J.-M. Lin, Y.-C. Hsu, J. Chem. Phys. 125 (2006) 133201.
[34] G.W. King, C.K. Ingold, Nature (London) 169 (1952) 1101.
[35] C.K. Ingold, G.W. King, J. Chem. Soc. (1953) 2702.
[36] K.K. Innes, J. Chem. Phys. 22 (1954) 863.
[37] J.K.G. Watson, M. Herman, J.C. Van Craen, R. Colin, J. Mol. Spectrosc. 95 (1982) 101.
[38] J.C. Van Craen, M. Herman, R. Colin, J.K.G. Watson, J. Mol. Spectrosc. 111 (1985) 185.
[39] A.L. Utz, J.D. Tobiason, E. Carrasquillo, L.J. Sanders, F.F. Crim, J. Chem. Phys. 98 (1993) 2742.
[40] J.D. Tobiason, A.L. Utz, F.F. Crim, J. Chem. Phys. 99 (1993) 928.
[41] A.H. Steeves, A.J. Merer, H.A. Bechtel, A.R. Beck, R.W. Field, Mol. Phys. 106 (2008) 1867.
[42] A.J. Merer, N. Yamakita, S. Tsuchiya, J.F. Stanton, Z. Duan, R.W. Field, Mol. Phys. 101 (2003) 663.
[43] A.J. Merer, N. Yamakita, S. Tsuchiya, A.H. Steeves, H.A. Bechtel, R.W. Field, J. Chem. Phys. 129 (2008) 054304.
[44] B.T. Darling, D.M. Dennison, Phys. Rev. 57 (1940) 128.
[45] I.M. Mills, Pure Appl. Chem. 11 (1965) 325.
[46] M. Herman, A. Campargue, M.I. El Idrissi, J. Vander Auwera, J. Phys. Chem. Ref. Data 32 (2003) 921.
[47] Y. Chen, S. Halle, D.M. Jonas, J.L. Kinsey, R.W. Field, J. Opt. Soc. Am. B 7 (1990) 1805.
[48] A.J. Merer, Z. Duan, R.W. Field, J.K.G. Watson, Can. J. Phys., in press.
[49] J.T. Hougen, J.K.G. Watson, Can. J. Phys. 43 (1965) 298.
[50] T.R. Huet, M. Godefroid, M. Herman, J. Mol. Spectrosc. 144 (1990) 32.
[51] J.H. Meal, S.R. Polo, J. Chem. Phys. 24 (1956) 1119.
[52] L. Hedberg, I.M. Mills, J. Mol. Spectrosc. 160 (1993) 117.
[53] K.K. Lehmann, Mol. Phys. 66 (1989) 1129.
[54] K.L. Bittinger, Ph. D. thesis, M.I.T., 2008.
[55] N. Ochi, S. Tsuchiya, Chem. Phys. 152 (1991) 319.